Novel square pyramidal iron(III) complexes of linear tetradentate bis(phenolate) ligands as structural and reactive models for intradiol-cleaving 3,4-PCD enzymes: Quinone formation *vs.* intradiol cleavage†

Ramasamy Mayilmurugan,[a] Muniyandi Sankaralingam,[a] Eringathodi Suresh[b] and Mallayan Palaniandavar*[a]

Received 18th March 2010, Accepted 14th July 2010
DOI: 10.1039/c0dt00171f

The iron(III) complexes of the bis(phenolate) ligands 1,4-bis(2-hydroxy-4-methyl-benzyl)-1,4-diazepane H_2(L1), 1,4-bis(2-hydroxy-4-nitrobenzyl)-1,4-diazepane H_2(L2), 1,4-bis(2-hydroxy-3,5-dimethylbenzyl)-1,4-diazepane H_2(L3) and 1,4-bis(2-hydroxy-3,5-di-*tert*-butylbenzyl)-1,4-diazepane H_2(L4) have been isolated and studied as structural and functional models for 3,4-PCD enzymes. The complexes [Fe(L1)Cl] **1**, [Fe(L2)(H_2O)Cl] **2**, [Fe(L3)Cl] **3** and [Fe(L4)Cl] **4** have been characterized using ESI-MS, elemental analysis, and absorption spectral and electrochemical methods. The single crystal X-ray structure of **3** contains the FeN_2O_2Cl chromophore with a novel square pyramidal (τ, 0.20) coordination geometry. The Fe–O–C bond angle (135.5°) and Fe–O bond length (1.855 Å) are very close to the Fe–O–C bond angles (133, 148°) and Fe–O(tyrosinate) bond distances (1.81, 1.91 Å) in 3,4-PCD enzyme. All the complexes exhibit two intense absorption bands in the ranges 335–383 and 493–541 nm, which are assigned respectively to phenolate (pπ) → Fe(III) (dσ*) and phenolate (pπ) → Fe(III) (dπ*) LMCT transitions. The Fe(III)/Fe(II) redox potentials of **1**, **3** and **4** ($E_{1/2}$, –0.882– –1.010 V) are more negative than that of **2** ($E_{1/2}$, –0.577 V) due to the presence of two electron-withdrawing *p*-nitrophenolate moieties in the latter enhancing the Lewis acidity of the iron(III) center. Upon adding H_2DBC pretreated with two equivalents of Et_3N to the iron(III) complexes, two catecholate-to-iron(III) LMCT bands (656, ε, 1030; 515 nm, ε, 1330 M^{-1} cm^{-1}) are observed for **2**; however, interestingly, an intense catecholate-to-iron(III) LMCT band (530–541 nm) is observed for **1**, **3** and **4** apart from a high intensity band in the range 451–462 nm. The adducts $[Fe(L)(DBC)]^-$ generated from **1–4** *in situ* in DMF/Et_3N solution react with dioxygen to afford almost exclusively the simple two-electron oxidation product 3,5-di-*tert*-butylbenzoquinone (DBQ), which is discerned from the appearance and increase in intensity of the electronic spectral band around 400 nm, and smaller amounts of cleavage products. Interestingly, in DMF/piperidine the amount of quinone product decreases and those of the cleavage products increase illustrating that the stronger base piperidine enhances the concentration of the catecholate adduct. The rates of both dioxygenation and quinone formation observed in DMF/Et_3N solution vary in the order **1** > **3** > **4** < **2** suggesting that the ligand steric hindrance to molecular oxygen attack, the Lewis acidity of the iron(III) center and the ability of the complexes to rearrange the Fe–O phenolate bonds to accommodate the catecholate substrate dictate the extent of interaction of the complexes with substrate and hence determine the rates of reactions. This is in line with the observation of DBSQ/H_2DBC reduction wave for the adduct $[Fe(L2)(DBC)]^-$ at a potential ($E_{1/2}$: –0.285 V) more positive than those for the adducts of **1**, **3** and **4** ($E_{1/2}$: –0.522 to –0.645 V).

Introduction

A number of important oxidative transformations are carried out by iron enzymes utilizing dioxygen as an oxygen source.[1–5] The oxidative cleavage of catechol and other dihydroxy aromatics is a key step in the biodegradation of naturally occurring aromatic molecules and many aromatic environmental pollutants by soil bacteria.[6,7] Catechol dioxygenases are a class of non-heme iron enzymes that catalyse the oxidative cleavage of catechols. They are divided into two subclasses: the intradiol dioxygenases, which utilize a non-heme iron(III) cofactor in catalyzing the cleavage of the carbon–carbon bond between the two catechol oxygens; and the extradiol dioxygenases, which utilize a non-heme iron(II) cofactor in catalyzing the cleavage of the carbon–carbon bond adjacent to the catechol oxygens.[8–17] Even though intradiol cleavage is the less common route in the biodegradation of aromatic molecules as compared to extradiol cleavage, extensive investigation of intradiol dioxygenases has been made due to the rich spectroscopy of the iron(III) active site in the enzymes.[14–16] The two most investigated enzymes of the intradiol dioxygenases are catechol 1,2-dioxygenase (1,2-CTD) and protocatechuate 3,4-dioxygenase (3,4-PCD). The iron(III) center in these enzymes adopts a trigonal bipyramidal geometry with two inequivalent tyrosine ligands (axial, Tyr447 and equatorial, Tyr408), two histidines (His460, His462), and a hydroxide ion.[10–18] On binding

[a]*Centre for Bioinorganic Chemistry, School of Chemistry, Bharathidasan University, Tiruchirapalli, 620 024, India. E-mail: palanim51@yahoo.com, palaniandavarm@gmail.com*
[b]*Analytical Science Discipline, Central Salt and Marine Chemicals Research Institute, Bhavnagar, –364 002, India*

† CCDC reference number 770712. For crystallographic data in CIF or other electronic format see DOI: 10.1039/c0dt00171f

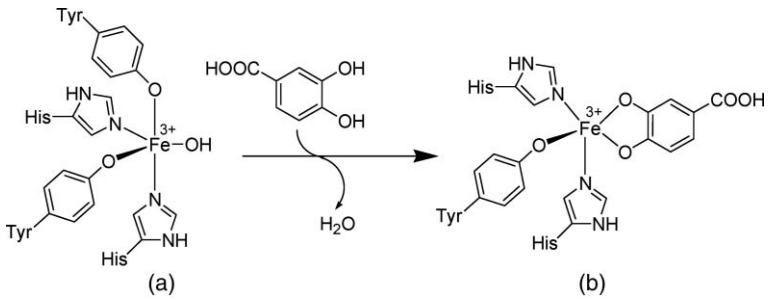

Scheme 1 Structures of active site of 3,4-PCD (a) and the 3,4-PCD-substrate adduct (b).

to iron(III) the catechol substrate (PCA) donates its hydroxyl protons to the hydroxide ligand and the axial tyrosine (Tyr447) to afford a bidentate iron(III) catecholate complex.[16,17] The active site geometry is converted into a square-pyramidal geometry and the axial Tyr447 and equatorial OH^- are displaced by the doubly deprotonated substrate and retains the endogenous histidine and equatorial tyrosine (Tyr408) ligands (Scheme 1).[10–18] The open coordination position is *trans* to His460, and the substrate chelates asymmetrically to the iron(III) center, with the longer bond *trans* to the equatorial Tyr408.[19] The asymmetric chelation of the substrate moiety is determined[19] by the Fe–O–C bond angle of equatorially bound tyrosinate in the 3,4-PCD enzyme–substrate complex, which in turn influences the extent of iron(III)-catecholate covalency and hence substrate activation for reaction with O_2.

The study of iron(III) complexes[18,20–30] of ligands with phenolate oxygen and pyridine nitrogen donors have provided valuable information to elucidate the structure–function correlation for the active site geometries of the intradiol-cleaving enzymes. The ligand donor functions in the complexes display different steric and electronic effects in determining the Lewis acidity of the iron(III) center and hence their intradiol cleavage activity. Recently we have reported[22,31] a few mononuclear iron(III) complexes of sterically hindering tetradentate tripodal monophenolate ligands, which closely mimic the enzyme active site structure and function. The complex $[Fe(L)Cl_2]$, where H(L) is *N*,*N*-dimethyl-*N*′-(pyrid-2-ylmethyl)-*N*′-(2-hydroxy-4-nitrobenzyl)ethylenediamine, exhibits a relatively high Fe–O–C bond angle of 136.1° and shows an enhanced rate of dioxygenation. Interestingly, upon replacement[22] of the *p*-nitrophenolate arm in this complex by a 3,5-dimethylphenolate arm to obtain the complex $[Fe(L)Cl_2]$, where H(L) is *N*,*N*-dimethyl-*N*′-(2-hydroxy-3,5-dimethylbenzyl)-*N*′-(pyrid-2-ylmethyl)ethylenediamine, the higher Fe–O–C bond angle (134.0°) is retained but a regioselective extradiol cleavage of 3,5-di-*tert*-butylcatechol (H_2DBC) is observed.[31]

Though the active site structures of intradiol-cleaving enzymes contain two tyrosine phenolate residues, only a few iron(III) complexes of bis(phenolate) ligands have been so far isolated and studied as functional models for the enzymes. Earlier Que *et al.* reported[32] the catecholate adducts of iron(III)-SALEN complexes and observed that the rates of oxygenation of the adducts are poor, and the main product obtained in the reaction is typically the two-electron oxidation product benzoquinone. Previously we observed[25b] that iron(III) complexes of bis(phenolate) ligands also elicit intradiol cleavage products with yields higher than those of iron(III) complexes of the corresponding monophenolate ligands. The structure of the novel complex $[Fe(Mes_6\text{-SALEN})(OH_2)]ClO_4$, where Mes_6-SALEN is bis(3,5-dimesitylsalicylidene)-1,2-dimesitylethylene-diamine, has been reported[33] to adopt distorted trigonal bipyramidal coordination geometry (τ, 0.48) as in the 3,4-PCD active site (τ, 0.44), but no reactivity studies on the complex were carried out. Krebs *et al.*[26,27] isolated several iron(III) complexes of substituted bis-phenolate ligands and studied them as models for the inhibitor-substrate adducts of intradiol-cleaving 1,2-CTD enzyme. This report describes novel iron(III) complexes of new sterically hindering diazepane-based linear bis-phenolate ligands [H_2(L1)–H_2(L4), Scheme 2] which not only closely mimic the coordination of two tyrosine phenolate donors in the active site of 3,4-PCD enzymes but also mimic their spectral properties and function. Such ligands with a 1,4-diazepane back bone are interesting because incorporation of this 1,4-diazepane moiety in a 4N ligand system confers a rare *cis*-β configuration on the iron(III) complex-catecholate adduct and elicits regioselective extradiol cleavage of catechol.[34] Also, we have very recently found[21] that incorporation of two 3,5-dimethylphenolate arms as in [Fe(L5)Cl] (Scheme 2) confers a distorted trigonal bipyramidal coordination geometry on iron(III), which is closely related to the trigonal bipyramidal iron(III) core in the substrate-free 3,4-PCD enzyme, but the complex fails to exhibit dioxygenase activity. In contrast, the analogous complex $[Fe(L6)(Cl)(H_2O)]$ exhibits an octahedral coordination geometry and shows, interestingly, intradiol cleavage activity. Similarly, the five-coordinate complex [Fe(L7)Cl] fails to cleave catechol while the octahedral complex $[Fe(L8)(Cl)(H_2O)]$ exhibits a very fast intradiol cleavage reaction.[21] Also, we have

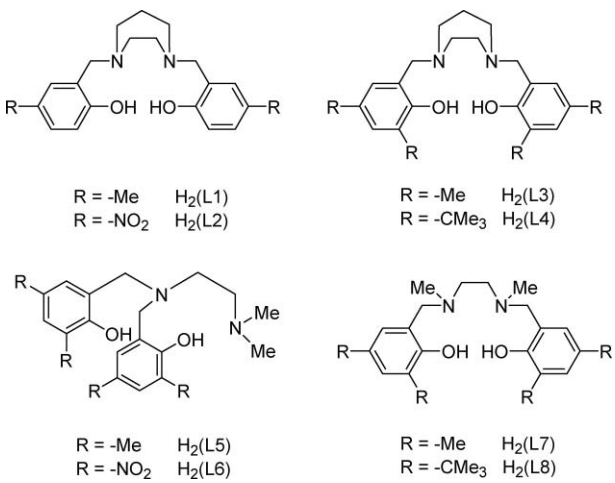

Scheme 2 Structures of linear and tripodal bis(phenolate) ligands.

now shown that the parent ligand 1,4-bis(2-hydroxybenzyl)-1,4-diazepane (H_2(L9)) forms the dimeric complex [Fe_2(μ-O)(L9)$_2$] in which each iron atom has a distorted square pyramidal coordination geometry (τ, 0.45).[35] So, it is expected that incorporation of different substituents with varying electronic and steric effects on the phenolate ring as in the present ligands would confer unusual coordination geometries on iron(III) and varying dioxygenase activities as well. Thus, the X-ray crystal structure of the present bis(phenolato)iron(III) complex [Fe(L3)Cl] with two 3,5-dimethylphenolate arms exhibit a novel square pyramidal coordination geometry with a Fe–O–C bond angle of 135.5°, which is close to that in the enzyme active site. Interestingly, the catecholate adducts of all the complexes in DMF–acetonitrile/triethylamine solution yield the two-electron oxidized product 3,5-di-*tert*-butylbenzoquinone almost exclusively with small amounts of catechol cleavage products. However, in DMF/piperidine solution decreased amounts of benzoquinone and enhanced amounts of intradiol cleavage products are observed.

Experimental section

Materials

Homopiperazine, 2-hydroxy-5-methylbenzaldehyde, 2,4-di-*tert*-butylphenol, 3,5-di-*tert*-butylcatechol (H_2DBC), 4-*tert*-butylcatechol (H_2TBC), 2,4-dimethylphenol, sodium cyanotrihydroborate, catechol (H_2CAT) and 4-nitrocatechol (H_2NCAT) (Aldrich) and iron(III) chloride (anhydrous) (Merck, India), 3,4,5,6-tetrachlorocatechol (H_2TCC, Lancaster) were used as received, unless noted otherwise and H_2DBC was recrystallized from hexane before use. The supporting electrolyte tetra-*N*-butylammonium perchlorate (NBu_4ClO_4, G. F. Smith, USA) was recrystallized twice from aqueous ethanol.

Physical measurements

Elemental analyses were performed on a Perkin Elmer Series II CHNS/O Analyzer 2400. ^{1}H NMR spectra were recorded on a Bruker 200 MHz NMR spectrometer. The electronic spectra were recorded on an Agilent diode array-8453 spectrophotometer. The EPR spectra were recorded on a JEOL JES-TE 100 X-band spectrometer. ESI-Mass spectrometry was performed on a Thermo Finnigan LCQ 6000 Advantage Max instrument. Cyclic voltammetry (CV) and differential pulse voltammetry (DPV) were performed using a three electrode cell configuration. A platinum sphere, a platinum plate and Ag(s)/Ag^+ were used as working, auxiliary and reference electrodes respectively. The supporting electrolyte used was NBu_4ClO_4 (TBAP). The temperature of the electrochemical cell was maintained at 25.0 ± 0.2 °C by a cryocirculator (HAAKE D8 G). By bubbling research grade nitrogen the solutions were deoxygenated and an atmosphere of nitrogen was maintained over the solutions during measurements. The $E_{1/2}$ values were observed under identical conditions for various scan rates. The instruments utilized included an EG & G PAR 273 Potentiostat/Galvanostat and Pentium-IV computer along with EG & G M270 software to carry out the experiments and to acquire the data. The product analyses were performed using a HP 6890 GC series Gas Chromatograph equipped with a FID detector and a HP-5 capillary column (30 m × 0.32 mm × 2.5 μm) and GC-MS analysis was performed on a Perkin Elmer Clarus 500 GC-MS instrument using a PE-5 with the previously[31] reported temperature program.

Synthesis of ligands

1,4-Bis(2-hydroxy-4-methylbenzyl)-1,4-diazepane H_2(L1). To a solution of 2-hydroxy-5-methylbenzaldehyde (1.36 g, 10.0 mmol) in methanol (50 mL) were added homopiperazine (0.50 g, 5.0 mmol) and a small amount of acetic acid. Sodium cyanotrihydroborate (0.63 g, 10.0 mmol) in methanol (5 mL) was added dropwise to the resulting solution with stirring. After the solution was stirred for 3 days at 25 °C, it was acidified by adding conc. HCl and then evaporated almost to dryness under a reduced pressure. The residue is dissolved in saturated aqueous Na_2CO_3 solution (50 mL) and extracted with $CHCl_3$ (3 × 50 mL). The combined extracts were dried over anhydrous Na_2SO_4 and filtered. Slow evaporation of the filtrate gives a white crystalline ligand H_2(L1). Yield: 0.84 g (49%). The ligand was further purified by recrystallization from CH_2Cl_2. mp: 110–112 °C. ^{1}H NMR (200 MHz, $CDCl_3$): δ 1.27 (s, 6H), 1.42 (s, 4 H), 1.95 (pentet, 2 H), 2.77 (t, 4 H), 3.77 (s, 4H), 6.82 (d, 2H), 7.21 (d, 2H), 7.21 (s, 2H).^{13}C NMR (360 MHz, C_6D_6): δ 20.91 (CH_3), 27.06, 53.50, 54.81, 62.28 (CH_2), 116.86, 122.29, 128.20, 129.74, 130.07, 156.97 (ArC).

1,4-Bis(2-hydroxy-4-nitrobenzyl)-1,4-diazepane H_2(L2). The synthesis of H_2(L2) was carried out in three steps. The first step in the synthesis of this compound involves preparation of methylal,[21,22] which was reacted with *p*-nitrophenol in the second step to obtain 2-hydroxy-5-nitrobenzyl chloride. The latter was then reacted with homopiperazine to yield H_2(L2).

To a solution of 2-hydroxy-5-nitrobenzyl chloride (1.50 g, 8 mmol) in tetrahydrofuran (30 mL) were added homopiperazine (0.40 g, 4 mmol) and triethylamine (0.81 g, 1.11 mL, 8 mmol). The mixture was refluxed for 2 h to give a yellow suspension which was cooled and filtered. The filtrate was rotaevaporated to give a yellow solid that was washed thoroughly with methanol and then used as such for synthesis of its complex. Yield: 0.87 g (54%). mp 148–150 °C. ^{1}H NMR (200 MHz, $CDCl_3$): δ 1.94 (pentet, 2 H), 2.81 (s, 4 H), 2.85 (t, 4 H), 3.85 (s, 4H), 6.84 (d, 2H), 8.03 (s, 2H), 8.07 (d, 2H). ^{13}C NMR (400 MHz, $CDCl_3$): δ 26.57, 53.71, 54.10, 61.28 (CH_2), 116.80, 121.51, 124.87, 125.74, 140.33, 164.59 (ArC).

1,4-Bis(2-hydroxy-3,5-dimethylbenzyl)-1,4-diazepane H_2(L3). A solution of 2,4-dimethylphenol (3.66 g, 30.0 mmol), homopiperazine (1.50 g, 15.0 mmol) and 37% aqueous formaldehyde (3.5 mL, 42.0 mmol) in methanol (10 mL) was stirred and refluxed for 24 h. The mixture was cooled and the product obtained was filtered off and washed with ice-cold methanol to give a colorless product. Yield: 4.20 g (76%). The product was purified by recrystallization from CH_2Cl_2. mp: 98–100 °C. ^{1}H NMR (200 MHz, $CDCl_3$): δ 1.89 (pentet, 2 H), 2.17 (s, 12H), 2.74 (s, 4 H), 2.79 (t, 4H), 3.70 (s, 4H), 6.83 (s, 2H), 6.58 (s, 2H), 7.23 (s, 2H, OH). ^{13}C NMR (360 MHz, $CDCl_3$): δ 15.56, 20.34 (CH_3), 26.46, 53.37, 54.36, 61.72 (CH_2), 120.63, 124.60, 126.61, 127.61, 130.62, 153.51 (ArC).

1,4-Bis(2-hydroxy-3,5-di-*tert*-butylbenzyl)-1,4-diazepane H_2(L4). A solution of 2,4-di-*tert*-butylphenol (5.0 g, 24.2 mmol), homopiperazine (1.21 g, 12.1 mmol) and 37% aqueous formaldehyde (2.5 mL, 33.6 mmol) in methanol (10 mL) was stirred and refluxed

for 24 h. The mixture was cooled and the product was filtered off and washed with ice-cold methanol to give a colorless product. Yield: 4.71 g (72%). The product was purified by recrystallization from CH_2Cl_2. mp: 173–175 °C. ^{1}H NMR (200 MHz, $CDCl_3$): δ 1.27 (s, 18 H), 1.42 (s, 18 H), 1.94 (pentet, 2H), 2.77 (s, 4 H), 2.82 (t, 4 H), 3.77 (s, 4H), 6.82 (s), 7.21 (s, 2H), 7.26 (s, 2H, OH). ^{13}C NMR (400 MHz, $CDCl_3$): δ 26.76, 29.61, 31.70 (CH_3), 34.15, 34.86, 53.07, 54.45 (CH_2), 62.45 (*tert*-C), 121.22, 123.01, 123.44, 135.66, 140.59, 154.29 (Ar–C).

Synthesis of complexes

[Fe(L1)Cl] 1. The complex [Fe(L1)Cl] **1** was prepared by adding of a solution of $FeCl_3$ (0.16 g, 1.0 mmol) in methanol (5 mL) to an acetonitrile solution (10 mL) of an equivalent amount of the ligand H_2(L1) (0.34 g, 1.0 mmol). The solution was stirred for an hour. The blue colored precipitate obtained was filtered off, washed with small amounts of cold methanol and dried *in vacuo* over P_4O_{10}. Yield: 0.18 g (42%). Anal. Calcd. for $C_{21}H_{26}N_2O_2FeCl$: C, 58.69; H, 6.40; N, 6.52. Found C, 58.72; H, 6.39; N, 6.53.

[Fe(L2)Cl(H_2O)] 2. This complex was prepared as a dark brown colored product by using the procedure employed for preparing complex **1**. Yield: 0.26 g (52%). Anal. Calcd. for $C_{19}H_{22}N_4O_7FeCl$: C, 44.77; H, 4.35; N, 10.99. Found C, 44.75; H, 4.38; N, 10.72. ESI-MS, *m*/*z*, 508.

[Fe(L3)Cl] 3. A methanolic slurry (4 mL) of the ligand H_2(L3) (0.37 g, 1.0 mmol) was treated with $FeCl_3$ (0.16 g, 1.0 mmol) in methanol (4 mL) and then triethylamine (0.20 g, 280 μL, 2.0 mmol) in methanol (2 mL) was added. The mixture was stirred for 30 min. The dark blue coloured precipitate obtained was filtered off, washed with small amounts of cold methanol and dried over P_4O_{10}. Yield: 0.33 g (72%). Anal. Calcd. for $C_{23}H_{30}N_2O_2FeCl$: C, 60.34; H, 6.60; N, 6.12. Found C, 60.30; H, 6.82; N, 6.3. The complex was recrystallized from hot acetonitrile to give a dark blue crystalline solid. The solid was refluxed in CH_3OH–CH_3CN (1 : 1) mixture for 10 min and upon cooling the solution at room temperature bright blue crystals suitable for X-ray diffraction were obtained.

[Fe(L4)Cl] 4. The complex **4** was prepared by the reaction of a methanolic (4 mL) slurry of the ligand H_2(L4) (0.54 g, 1.0 mmol) with $FeCl_3$ (0.16 g, 1.0 mmol) in methanol (4 mL) in the presence of Et_3N (0.20 g, 280 μL, 2.0 mmol) in methanol (2 mL). The mixture was stirred for 30 min. The dark blue crystalline precipitate obtained was filtered off, washed with small amounts of cold methanol and dried over P_4O_{10}. Yield: 0.49 g (78.72%). Anal. Calcd. for $C_{35}H_{54}N_2O_2FeCl$: C, 67.14; H, 8.69; N, 4.47. Found C, 67.16; H, 8.62; N, 4.50.

Kinetics and reactivity studies

Kinetic analyses[21–29,31] of the catechol cleavage reactions were carried out by time-dependent measurement of the disappearance of the lower energy DBC^{2-}-to-iron(III) LMCT band at ambient temperature (25 °C) by exposing to molecular oxygen. The solvents were equilibrated at the atmospheric pressure of O_2 at 25 °C and the solubility of O_2 at 25 °C is: acetonitrile, 8.1×10^{-3} M;[28,36] DMF (dimethylformamide), 4.86×10^{-3} M.[36,37]

Table 1 Crystal data and structure refinement for [Fe(L3)Cl] **3**

Empirical formula	$C_{23}H_{29}ClFeN_2O_2$
FW	456.78
Crystal system	Orthorhombic
Space group	*Cmc*21
a/Å	20.257(2)
b/Å	15.3291(17)
c/Å	7.3121(8)
$\alpha = \beta = \gamma$ (°)	90
V/Å^3	2270.5(4)
T/K	273(2)
Mo-Kα λ, (Å)	0.71073
density/Mg m^{-3}	1.336
Z	4
μ/mm^{-1}	0.802
F(000)	960
no. of reflections collected	6558
Goodness-of-fit on F^2	1.144
R_1[a]	0.0522
wR_2[b]	0.1350

[a] $R1 = \sum\|F_o\| - |F_c\|/\Sigma\,|F_o|$, [b] $wR2 = \sum w\{(F_o^2 - F_c^2)^2/\Sigma w\,[(F_o^2)^2]\}^{1/2}$

The dioxygenase activities of the present complexes were determined using a known[22,31,34] procedure with modifications. The complex (0.1 mmol), H_2DBC (0.022 g, 0.1 mmol), and Et_3N (0.20 g, 28 μL, 0.2 mmol) were dissolved in DMF (5 mL) and exposed to dioxygen and stirred for 48 h. The oxygenation reaction was quenched by the addition of 6 M HCl solution (5 mL). The products were extracted from the aqueous solution with diethyl ether (3 × 30 mL). The clear yellow organic layer was separated, washed twice with 2 M HCl (20 mL) and then dried over anhydrous Na_2SO_4 at room temperature and then filtered off and the combined filtrate was evaporated *in vacuo*, which yields the products. The products were analyzed by GC-MS (EI) and quantified by GC (FID). The cleavage products were quantified by comparing the GC retention times of the reaction products with those of authentic samples prepared by using iron(III) complexes reported by us previously.[31,34]

Single-crystal X-ray data collection and structure solution

A single crystal of **3** of suitable size was selected from the mother liquor and immersed in paraffin oil, then mounted on the tip of a glass fiber and cemented using epoxy resin. Intensity data for the crystal were collected using Mo-Kα ($\lambda = 0.71073$ Å) radiation on a Bruker SMART APEX diffractometer equipped with a CCD area detector at 273 K. The crystallographic data are collected in Table 1. The SMART[38] program was used for collecting frames of data, indexing reflection, and determination of lattice parameters; SAINT[38] program for integration of the intensity of reflections and scaling; SADABS[39] program for absorption correction, and the SHELXTL[40] program for space group and structure determination, and least-squares refinements on F^2. The structure was solved by heavy atom method. Other non-hydrogen atoms were located in successive difference Fourier syntheses. The final refinement was performed by full-matrix least-squares analysis. Hydrogen atoms attached to the ligand moiety were located from the difference Fourier map and refined isotropically.

Results and discussion

Synthesis and characterization of ligands and complexes

The present ligands were synthesized according to known procedures,[21,35,41] which involve Mannich condensation, reductive amination and simple substitution reactions, with suitable modifications. The amino hydrogens in homopiperazine have been replaced with differently substituted phenolate moieties to generate the ligands (Scheme 2) for the present study. The tetradentate ligand H_2(L1) was synthesized by the reductive amination of 2-hydroxy-5-methylbenzaldehyde using sodium cyanotrihydroborate as the reducing agent.[35] The ligand H_2(L2) was synthesized[21] by substitution reaction of homopiperazine with 2-hydroxy-5-nitrobenzyl chloride. The ligands H_2(L3) and H_2(L4) were synthesized[41] in good yields by the reaction of the Mannich base formed *in situ* by *ortho* and *para* substituted phenols using excess of 37% aqueous formaldehyde. The N_2O_2 donor set of the present ligands mimics the metal coordinating side chains of amino acids (histidine and tyrosinate residues) in 3,4-PCD enzymes. The two phenolate [pK_a (BH^+): phenol, 9.95] arms with electron-releasing methyl and *tert*-butyl and electron-withdrawing -NO_2 groups in the ligands are expected not only to duplicate tyrosinate residues in the active site but also mimic the function of 3,4-PCD. The methyl and *tert*-butyl substituents have been introduced not only to tune the spectral and electrochemical properties but also to effect a variation in reactivity of the model complexes by providing steric hindrance to O_2 attack. The 2,4-disubstituted phenolate moiety has been shown[21,33] to favor the formation of monomeric five-coordinate complexes but with varying structural, spectral and electrochemical properties. The reaction of $FeCl_3$ and the bis-phenolate ligands in the presence of two equivalents of Et_3N results in the immediate formation of the complexes. The complexes **1**, **3** and **4** are formulated as [Fe(L)Cl], which is supported by the X-ray crystal structure of one of them (**3**, *cf.* below), while **2** is formulated as [Fe(L2)(Cl)(H_2O)] based on the ESI-MS and elemental analysis. Attempts to grow single crystals of the latter were unsuccessful. The conductivities of all the bis-phenolate complexes (Λ_M, 6–13 Ω^{-1} cm^2 mol^{-1}) suggest that the chloride ion is certainly coordinated in acetonitrile solution.[22–25] The five-coordinate complexes **1**, **3** and **4** containing only one coordinated chloride ion may expand the coordination sphere to accommodate the bidentate catecholate substrates. All the iron(III) complexes have magnetic moments in the range 5.6–5.8 BM at room temperature, which is characteristic of a high-spin ferric center with five unpaired electrons.[22-29,31] The catecholate adducts of the iron(III) complexes were generated in solution for spectral and reactivity studies.

Description of the X-ray crystal structure of [Fe(L3)Cl] 3

The molecular structure of complex **3**, which looks like a butterfly, is depicted in Fig. 1 together with the atom numbering scheme. The selected bond lengths and bond angles are collected in Table 2. The coordination environment around the iron atom is described as distorted square pyramidal with the trigonality index[42] τ of 0.20 [$\tau = (\beta-\alpha)/60$, where β = O1–Fe–N1a = 147.62° and α = C1–O1–Fe = 135.5°; for perfect square pyramidal and trigonal bipyramidal geometries the τ values are zero and unity respectively]. The two phenolate oxygens and two tertiary amine nitrogens of the bisphenolate ligand are bonded to iron(III) at the four corners of the basal plane of the square pyramid and the chloride ion occupies the apical site. The observed Fe–$O_{phenolate}$ bond distances are equal (Fe–O, 1.855 Å) and are nearly identical to the Fe–O_{tyr} bond distances in 3,4-PCD enzymes (Fe–O_{tyr447} (axial), 1.91 Å, Fe–O_{tyr408} (equatorial), 1.81 Å).[15,16,19] However, the Fe–$O_{phenolate}$ bond length in **3** is shorter than the average octahedral Fe–O bond distance[21–23,31,33] of ~1.92 Å, which is consistent with the high molar absorptivity of the $PhO^- \rightarrow$ Fe(III) LMCT band around 541 nm (*cf.* below). This illustrates that the pπ orbital of phenolate oxygen atom interacts[43] strongly with the half-filled dπ* orbital of iron(III) in the complex. The Fe–Cl bond distance (2.247 Å) falls within the range[21,33] for the five-coordinate iron(III) complexes suggesting that the chloride ion is less likely to be labile in solution (*cf.* above). The Fe–N_{amine} bond distance (2.202 Å) is almost close to the Fe–N_{his} bond distance in 3,4-PCD enzyme[15,19] (Fe–N_{His462}, 2.26, Fe–N_{His460}, 2.33 Å) but is shorter than that in five-coordinate bis-phenolate iron(III) complexes[21] and the average Fe^{III}–N bond distance (~2.15 Å) observed for octahedral iron(III) complexes.[21–26,31] The Fe–O–C bond angle (Fe–O1–C1, 135.5°) is also close to that in 3,4-PCD enzyme[15,19] (Fe–O–C_{tyr408}, 133 (equatorial); Fe–O–C_{tyr447} 148° (axial)). It is closer to that in octahedral iron(III) complexes of monophenolate ligands[22,31] with sterically demanding -NMe_2 group but it is much higher than those in octahedral iron(III) complexes of tripodal monophenolate ligands (~128.5°).[22,25b] It has been argued that the magnitude of this angle is a key factor to elicit catechol dioxygenase activity in intradiol-cleaving enzymes[19] and their model complexes.[22,31]

The square pyramidal coordination geometry of **3** is similar to that of the complex [Fe(Mes_6-SALEN)(Cl)] **10** reported by Fujii *et al.*[33] The Fe–N_{amine} bond distance in **3** (2.202 Å) is longer than the Fe–N_{imine} bond distance in **10** (2.087, 2.102 Å),

Table 2 Selected bond lengths[a] [Å] and bond angles[a] [deg] for [Fe(L3)Cl] **3**

Fe(1)–N(1)	2.202(4)
Fe(1)–O(1)	1.855(3)
Fe(1)–Cl(1)	2.2470(18)
O(1a)–Fe(1)–O(1)	98.2(2)
O(1)–Fe(1)–N(1)	87.26(14)
O(1)–Fe(1)–N(1a)	147.62(16)
N(1a)–Fe(1)–N(1)	72.36(18)
O(1)–Fe(1)–Cl(1)	107.45(12)
N(1)–Fe(1)–Cl(1)	101.13(11)
C(1)–O(1)–Fe(1)	135.5(3)

[a] Standard deviations in parenthesis.

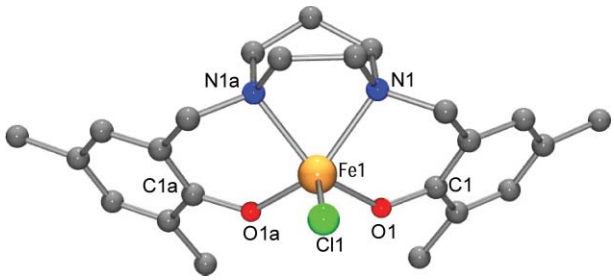

Fig. 1 Molecular structure of complex [Fe(L3)(Cl)] **3** (40% probability factor for the thermal ellipsoid). Hydrogen atoms have been omitted for clarity.

which is expected of sp^3 and sp^2 hybridizations[44] respectively of the tertiary amine and imine nitrogen atoms. However, the Fe–$O_{phenolate}$ bond distance in **3** (1.855 Å) is shorter than that in **10** (1.881 Å) suggesting that the iron-oxygen overlap in the former is stronger. Interestingly, on replacement of the chloride ion in **10** by a water molecule to obtain [Fe(Mes_6-SALEN)(OH_2)](ClO_4) a structural change from preferred square pyramidal to distorted trigonal bipyramidal geometry (τ, 0.48) is observed and the latter resembles that found in the active site (τ, 0.44) of 3,4-PCD enzyme in the resting state. So, it is expected that substitution of chloride ion in **3** by a water molecule would lead to a structural change from square pyramidal to a distorted trigonal bipyramidal geometry as in 3,4-PCD enzyme. It is to be noted that the five-coordinate iron(III) complex [Fe(L5)Cl] possesses a trigonal bipyramidal coordination geometry (τ, 0.79)[21] and closely resembles the iron(III) coordination environment of the 3,4-PCD enzyme active site. Further, the coordination geometry around each iron atom in [Fe_2(μ-O)($L9)_2$] with a Fe–O–Fe core is distorted square pyramidal (τ, 0.45) with the two amine nitrogen and two phenolate oxygen atoms of the ligand constituting the corners of the square plane and the μ-oxo oxygen atom (O3) occupying the axial position.[35] A square-pyramidal coordination geometry similar to **3** is suggested for the analogous complexes **1** and **4** based on stoichiometry and spectral properties (*cf.* below). On the other hand, the complex [Fe(L2)(Cl)(H_2O)] **2** is proposed to have an octahedral coordination geometry in which the tetradentate ligand L2 occupies the four equatorial sites around iron(III) and the chloride ion and water molecule occupy the two labile sites *trans* to each other. A similar coordination structure has been proposed[34] for the complex [Fe(L)Cl_2]Cl, where L is the linear ligand 1,4-bis(2-pyridylmethyl)-1,4-diazepane.

Electronic absorption and EPR spectra

All the bis(phenolate) complexes exhibit two intense LMCT bands (493–551, 327–501 nm, Table 3) in DMF solution. While the low energy band is assigned to the charge transfer transition from the pπ orbital (HOMO) of the phenolate ion to the half-filled dπ* orbital of iron(III), the high energy band is assigned to the charge transfer transition from the pπ orbital (HOMO) of the phenolate oxygen to the half-filled d-orbital of iron(III) (dσ*).[19,21,22,45] The more intense band observed in the range 200–284 nm is assignable to ligand-based transitions. Interestingly, the bands observed for **1**, **3** and **4** in DMF solution are higher in energy than those (517–541, 335–339 nm, Fig. 2, Table 3) in acetonitrile solution. It is well known that addition of a base increases the negative charge built on iron(III) leading to a raising in energy of the iron(III) d-orbitals and thus shifts the phenolate-to-iron(III) LMCT band to higher energies with or without change in absorptivity.[25] So it is suggested that DMF is coordinated to the iron(III) center of the complexes. The energy of the low energy LMCT band in DMF varies in the order **1** > **3** ≈ **4** > **2** reflecting the effect of phenolate ring substituents on the Lewis acidity of the iron(III) center. The incorporation of an electron-releasing methyl group at the *ortho* position of the phenolate ring in **1** to obtain **3** would be expected to raise[25a] the energy of the POMO orbital of the phenolate moiety and hence lead to a decrease in energy of the lowest energy phenolate (pπ) to iron(III) (dπ*) LMCT band.[19] A similar decrease in LMCT band energy is observed on replacing the methyl groups in **3** by *tert*-butyl groups to give **4**. Also, replacement of the electron-releasing methyl group on the phenolate moiety in **1** by the electron-withdrawing nitro group to give **2** would be expected to lower[25a] the energy of the POMO orbital of the phenolate moiety and hence lead to a lower energy for the lowest energy phenolate(pπ)-to-iron(III) (dπ*) LMCT band. The sensitivity of the band positions as well as their intensities to the iron(III) environment, that is the nature of the ligand donor functionalities, is reminiscent of the spectral features observed for the native CTD and PCD enzymes.[19]

When H_2DBC pretreated with two equivalents of Et_3N is added to [Fe(L2)(Cl)(H_2O)] **2** in DMF two well-defined bands (656, 515 nm) are observed, which are assignable to DBC^{2-}-to-Fe(III) LMCT transitions[21–29,31] involving two different catecholate orbitals on the chelated DBC^{2-}. A similar observation of two catecholate-to-iron(III) LMCT bands has been made for the catecholate adducts of iron(III) complexes of tridentate 3N,[23,44] tetradentate 4N[28,34,37] and monophenolate ligands.[22,31] The high energy DBC^{2-}-to-Fe(III) LMCT band would have merged with

Table 3 Electronic spectral data λ_{max}, nm (ε, M^{-1} cm^{-1}) for iron(III) complexes[a] and their adducts in acetonitrile–DMF solution

Solvent	Added catechols[b]	Fe(L1)Cl]	[Fe(L2)-(H_2O)Cl]	[Fe(L3)Cl]	[Fe(L4)Cl]
CH_3CN	None	517 (1 960) 335 (2 700) 283 (5 100) 238 (5 630) 200 (14 530)	—	541 (3 180) 335 (3 880) 284 (6 610) 239 (7 140)	540 (7 670) 339 (9 650) 282 (15 180) 241 (16 740)
	DBC^{2-}	548 (2 050) 468 (2 340) 375 (2 410) 213 (sh)	—	540 (5 380) 412 (4 910) 333 (sh) 286 (sh)	645 (7 320) 341 (3 020) 309(4300) 277 (8 450)
	TBC^{2-}	533 (1 810) 331 (3 450) 284 (6 700) 545 (19 980)	—	505 (5 640) 332 (8 840) 282 (16 570)	636 (2 680) 430 (18 780) 374 (sh) 304 (10 280)
	TCC^{2-}	516 (2 880) 307 (sh) 304 (10 070)	—	502 (5 600) 332 (sh) 282 (17 030)	575 (2 730) 491 (sh) 425 (19 990)
DMF	None	493 (3 000) 327 (6 000) 288 (11 320)	499 (3 530) 383 (7 640) 345 (9 650) 238 (16 980)	536 (3 010) 329 (6 760) 284 (11 520)	551(sh) 501(3 820) 326 (6 730) 288 (11 100)
	DBC^{2-}	530 (2 950) 462 (3 140) 332 (sh) 292 (14 160)	656 (1 030) 515 (1 330) 300 (8 780)	541 (2 980) 451 (3 330) 331 (7 190) 287(15 850)	539 (3 130) 451 (3 950) 375 (4 630)
	TBC^{2-}	—	513 (2 160) 337 (sh) 287 (9 110)	523 (3220) 330(sh)	504 (2870) 327(5330)
	TCC^{2-}	—	499 (2 850) 305 (7 490) 264 (sh)	508 (4490) 329(sh)	489 (3660) 335(sh) 305(sh)

[a] Concentration of iron(III) complexes, 2×10^{-4} M. [b] The ratio of added ligand to iron complexes was 1 : 1; the anions were generated by adding 2 equivalents of triethylamine.

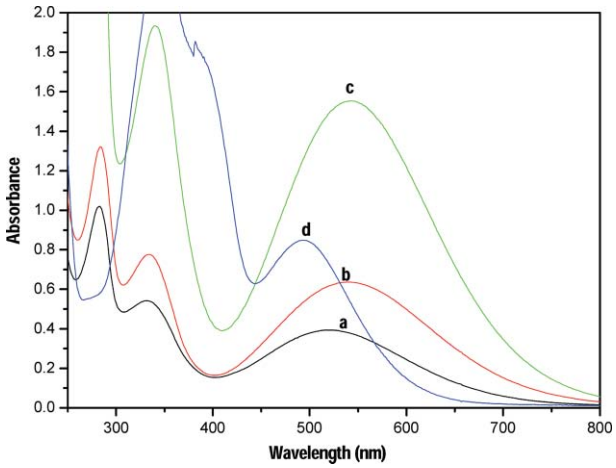

Fig. 2 Electronic absorption spectra of iron(III) complexes (2.0×10^{-4} M) in acetonitrile [Fe(L1)Cl] (a); [Fe(L3)Cl] (b); [Fe(L4)Cl] (c) and [Fe(L2)Cl(H_2O)] (d) in DMF solution, 1.0×10^{-4} M.

the intense phenolate-to-iron(III) LMCT band observed for **2** around 499 nm, which is now blue-shifted[21] to lower energy upon adduct formation. It is evident that upon adding the catecholate dianion to **2** the sterically constrained linear tetradentate ligand H_2(L2) rearranges[21,34] itself to provide *cis*-coordination positions for bidentate coordination of the catecholate dianion (Fig. 3). A similar rearrangement of the related linear 4N ligand 1,4-bis(2-pyridinylmethyl)-1,4-diazepane (L) coordinated to iron(III) to give a *cis*-β configuration has been established in the X-ray crystal structure of the adduct $[Fe(L)(TCC)]^+$, where TCC^{2-} is tetrachlorocatecholate.[34] In order to understand the adduct formation in more detail **2** was treated with one equivalent of H_2DBC, an increasing amount of piperidine or Et_3N was added and the changes in spectra are observed. Only very small spectral changes were observed upon adding the catechol to the complex suggesting negligible interaction of catechol with the complex. This is expected because when H_2DBC is added to [Fe(L)Cl_3] (L = tridentate 3 N ligand) or [Fe(L)Cl_2] (L = tridentate monophenolate ligand) two DBC^{2-} bands appear even in the absence of a base suggesting spontaneous deprotonation of H_2DBC upon interaction with the highly Lewis acidic iron(III) center. Upon adding increasing amounts of the strong base piperidine the intensity of the shoulder at 515 nm decreases and a new sharp band around 656 nm appears and starts growing in intensity. When the absorbance of the 515 nm feature is plotted as a function of number of equivalents of piperidine, a sharp inflexion is observed at one equivalent of base (Fig. 4). However, interestingly, when the absorbance of the 656 nm band is plotted, two inflexions are noted around one and two equivalents of piperidine. Similar results are obtained when Et_3N is used as the base; however, more than one equivalent but less than two equivalents of the weaker base is needed to obtain the inflexion

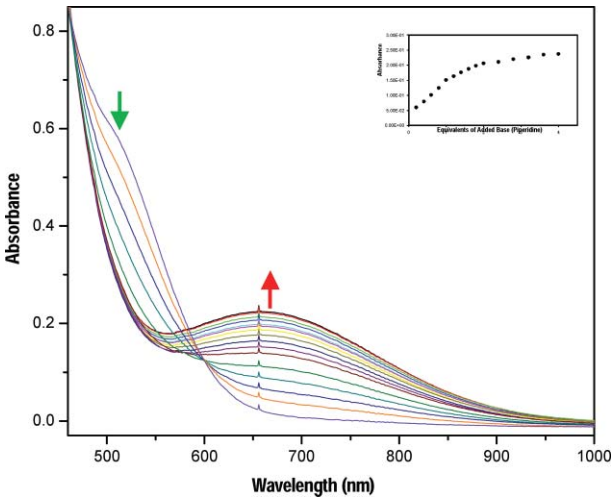

Fig. 4 Electronic absorption spectral changes observed during addition of piperidine to [Fe(L2)(H_2O)Cl] **2** (2×10^{-4} M) and H_2DBC (2×10^{-4} M) mixture in DMF. Inset: Plot of absorbance *vs* number of equivalents of added base at 656 nm.

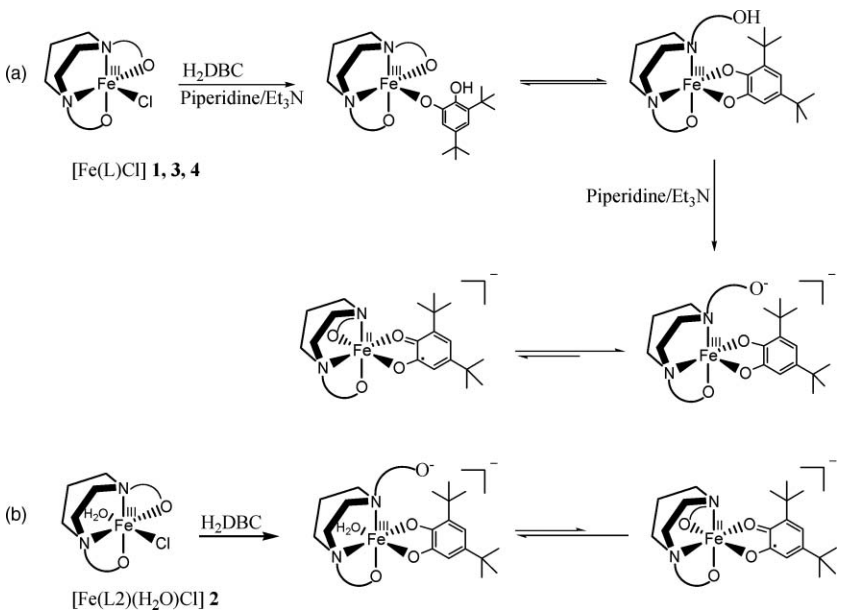

Fig. 3 Schematic illustration of mono- (a) and bidentate coordination of DBC^{2-} to iron(III) center.

for the changes in 515 nm band and only one well-defined inflexion but at two equivalents of base is observed for the disappearance of the 656 nm band (Fig. 4). So it is clear that the adduct species [Fe(L2)(HDBC)] in which $HDBC^-$ is coordinated in bidentate fashion to iron(III) and/or [Fe(L2)(HDBC)(H_2O)] in which $HDBC^-$ is monodentatively coordinated, is formed in DMF solution and that this species reacts with one more equivalent of piperidine to form the species $[Fe(L2)(DBC)]^-$ in which DBC^{2-} is coordinated in bidentate fashion.

In contrast to **2**, when H_2DBC pretreated with two equivalents of Et_3N is added to **1** both in DMF and acetonitrile solutions, a less intense broad band around 462 (DMF)/468 nm (CH_3CN) appears along with a low energy broad band, which corresponds to the DBC^{2-}-to-iron(III) LMCT bands[21,31] (Table 3). The intense phenolate-to-iron(III) LMCT band observed for **1** around 530 (DMF)/548 nm (CH_3CN) appears to have merged[21] with the high energy DBC^{2-}-to-Fe(III) LMCT band. Similar observations are made for the addition of DBC^{2-} to **3** with the appearance of a shoulder around 412 nm and a low energy band with low (DMF) or high (CH_3CN) intensity. The adduct formation of [Fe(L3)Cl] is followed by monitoring the decrease in intensity of the phenolate-to-iron(III) LMCT band around 535 nm and the growth of the high energy catecholate to iron(III) LMCT band around 451 nm as well, two inflexions at one and two equivalents of piperidine but only one but less well defined inflexion at two equivalents of Et_3N is observed. Upon adding DBC^{2-} to **4** in both CH_3CN and DMF a band around 451 nm with a low energy shoulder around 539 nm are observed revealing the catecholate adduct formation. When **4** is treated with one equivalent of H_2DBC, and then an incremental amount of the bases are added, the changes observed for the disappearance of the 499 nm band are found to be small, and only one but less well-defined inflexion at two equivalents of base is observed when the growth of the shoulder around 375 nm is monitored. It is obvious that bidentate coordination of DBC^{2-} to iron(III) complexes of the linear bis(phenolate) ligands H_2(L1)–H_2(L4) to give six-coordinate adducts with *cis*-β configuration (*cf.* above) would involve breaking of a Fe–$O_{phenolate}$ bond, followed by ligand rearrangement, and formation of a Fe–$O_{phenolate}$ bond.[31] Such a geometrical rearrangement in **2** would be more facile than in **1**, **3** and **4** as the electron-withdrawing *p*-nitro substituent in **2** would render the Fe–$O_{phenolate}$ bond weaker. Upon incorporation of one more methyl group in **1** to obtain **3** the Fe–$O_{phenolate}$ bonds become stronger (*cf.* below), illustrating the lower ability of the latter complex to form catecholate adducts. And upon replacing the methyl substituents in **3** by the more electron-releasing *tert*-butyl substituents on the phenolate rings to obtain **4** the Fe–$O_{phenolate}$ bond becomes much stronger illustrating the enhanced reluctance of the complex to form catecholate adducts. Thus structural changes from square pyramidal to octahedral geometry to accommodate the bidentatively coordinated DBC^{2-} would be more difficult than simple substitution reactions in octahedral complexes.[31] Molecular model building studies reveal that the re-coordination of the displaced phenolate oxygen in the vacant axial position is not facile, particularly for **4**. So, it is evident that monodentate coordination of the substrate (DBC^{2-}) by replacing the axially coordinated chloride ion followed by weaker coordination of the other catecholate oxygen would occur (Fig. 3) and hence an equilibrium between mono- and bidentatively coordinated adducts may be present in solution (*cf.* below).

Further, the energies of both the DBC^{2-}-to-Fe(III) LMCT bands of the adducts $[Fe(L)(DBC)]^-$ decrease along the series $[Fe(L1)(DBC)]^- > [Fe(L3)(DBC)]^- > [Fe(L2)(DBC)]^-$ revealing a remarkable dependence of the bands on the nature of the primary ligands[21–29] and reflecting the decrease in Lewis acidity of the iron(III) center of the adducts along this series, as modified by ligand substituents. Thus incorporation of the electron-withdrawing nitro group would tend to stabilize the dπ* orbital and hence decrease the energy gap between the metal orbital and the DBC^{2-} orbital leading to a lower energy for the catecholate-to-iron(III) LMCT band.[21,25a] In contrast, the electron-releasing methyl groups would destabilize the dπ* orbital leading to a higher energy for the LMCT band. Also, the position of the low energy catecholate → Fe(III) LMCT band in the complex-substrate adducts $[Fe(L)(catecholate)]^-$ generated from [Fe(L)Cl] is found to be shifted to lower energies as the substituents[21–25,31,46] on the catecholate ring are varied from electron-releasing to electron-withdrawing as observed previously: $TCC^{2-} > TBC^{2-} > DBC^{2-}$. This is expected as the electron-releasing substituents on the catecholate ring would decrease while electron-withdrawing substituents enhance the position of the low energy band,[21–25,31,46] thus reflecting the importance of electronic effects provided by the substituents on catechols.

It may be noted that the structure of the mono(μ-O)diiron(III,III) complex of the parent ligand of L1 has been determined.[35] In order to show that the complexes do not dimerize under the conditions of catecholate adduct formation the DMF solutions of the complexes were treated with increasing amounts of the bases and the spectral changes monitored. The color of solution changed from violet to red–orange. Interestingly, inflexions are observed at one and two equivalents of added base both for the disappearance of the phenolate-to-LMCT band and for the growth of the band around 427 nm for [Fe(L3)Cl] and that around 501 nm (Fig. 5) for [Fe(L4)Cl] suggesting the formation of a dimer with the Fe_2O core in two steps as follows:

$$[Fe^{III}(L)Cl] + H_2O \rightarrow [Fe^{III}(L)(H_2O)] + Cl^-$$

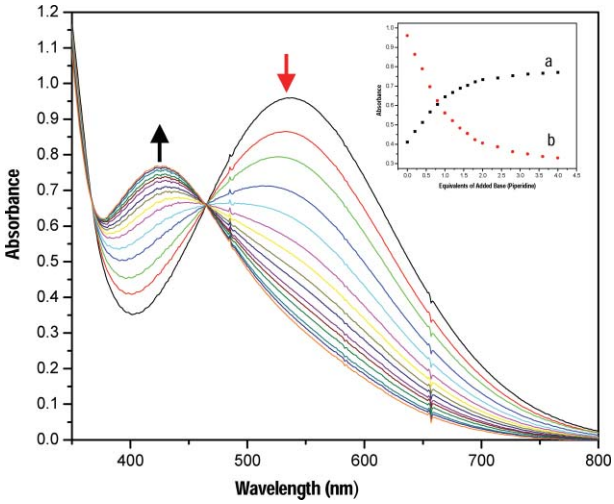

Fig. 5 Electronic absorption spectral changes observed during addition of piperidine to [Fe(L3)Cl] **3** in DMF. Inset: Plot of absorbance *vs* number of equivalents of added base for the formation of the absorption band around 427 nm (a) and disappearance of the band around 540 nm (b).

Table 4 EPR spectral data for iron(III) complexes in methanol/acetone solution at 77 K

Compound	*g* values	*E*/*D*
[Fe(L1)Cl]	8.70, 4.10, 2.10 4.80[a], 2.01, 1.99,1.89	0.095
[Fe(L2)Cl(H_2O)][b]	8.22, 4.01, 4.83[a]	0.087
[Fe(L3)Cl]	9.03, 4.09, 2.0 4.90, 1.95	0.10
[Fe(L4)Cl]	8.50, 4.10, 2.10 5.0[a], 2.01, 1.99, 1.98,1.88	0.092

[a] Minor component. [b] DMF/acetone solution.

$$[(L)Fe^{III}\text{-}OH_2] + Pip \rightleftharpoons [(L)Fe^{III}\text{-}OH] + PipH^+$$

$$[(L)Fe^{III}\text{--}OH + HO\text{--}Fe^{III}(L)] \xrightarrow{PiP} [(L)Fe^{III}\text{--}O\text{--}Fe^{III}(L)] + H_2O$$

The frozen solution EPR spectra of all the complexes display high-spin (S = 5/2) rhombic ferric signals[31,33,46] at *g* = 8.22–9.03, 4.01–4.10 (Fig. 6, Table 4) and 2.0–2.1 (*E*/*D*, 0.087–0.100) associated with the $|5/2, -1/2> \rightarrow |5/2, +1/2>$ transition and also signals corresponding to rhombic low-spin[47,48] (S = 1/2) iron(III) species (*g*, 4.8, 2.01, 1.99, 1.89). Upon replacing the two electron-releasing *p*-methylphenolate arms in **1** (g, 8.70; *E*/*D*, 0.095) by the electron-withdrawing *p*-nitrophenolate arms to obtain **2** a remarkable decrease in both the *g* value (8.22) and rhombicity (*E*/*D*, 0.087) is observed, which is consistent with the change in coordination geometry from square pyramidal to octahedral. In contrast, on incorporation of the methyl groups at *ortho* positions of the ligand in **1** to obtain **3** an appreciable increase in *g* value (9.03) and rhombicity (*E*/*D*, 0.10) is observed. This suggests that stronger Fe–O bond formation (*cf.* below) followed by an increase in steric constraint at the iron(III) center leads to an increase in *g* value and rhombicity. Also, on substituting the methyl groups in the ligand in **3** by *tert*-butyl groups to obtain **4** an appreciable decrease in *g* value (8.50) and rhombicity (*E*/*D*: **3**, 0.100; **4**, 0.092) is observed. This suggests that stronger coordination of the more basic bis-phenolate ligand H_2(L4) (*cf.* below) offsets the steric constraint at the iron(III) center and confers a less rhombic coordination environment on iron(III).

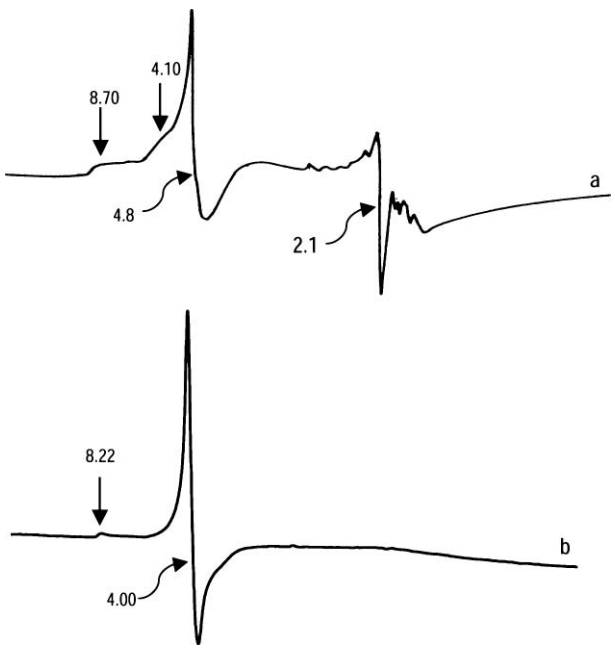

Fig. 6 EPR spectra of the iron(III) complexes [Fe(L1)Cl] **1** (a) and [Fe(L2)(H_2O)Cl] **2** (b) in frozen acetonitrile/acetone and DMF/acetone solutions respectively at 77 K.

Electrochemical properties

The redox behavior of the iron(III) complexes and their catecholate adducts generated *in situ* was studied by employing Cyclic Voltammetry (CV) and Differential Pulse Voltammetry (DPV) on a stationary platinum sphere as working electrode. The electrochemical responses of the complexes are well-behaved in DMF but not in acetonitrile. All the complexes exhibit a cathodic (–0.624 to –1.164 V) as well as an anodic wave (–0.540 to –0.996 V, Table 5, Fig. 7, 8) in DMF. The cathodic current functions (*D*, 1.0–3.2 × 10^{-6} cm^2 s^{-1}) calculated by substituting the slope obtained from the linear i_{pc} *vs.* $v^{1/2}$ ($v < 0.5$ Vs^{-1}) plot in the Randles–Sevcik's equation[49] are of the same order as those observed for other iron(III) complexes undergoing a one-electron reduction process.[22–25,31] The $E_{1/2}$ values of the Fe(III)/Fe(II) redox couple of the complexes follow the trend **2** > **1** > **3** > **4**. On replacing the electron-releasing methyl groups on the phenolate arms in **1** by the electron-withdrawing nitro groups as in **2** the

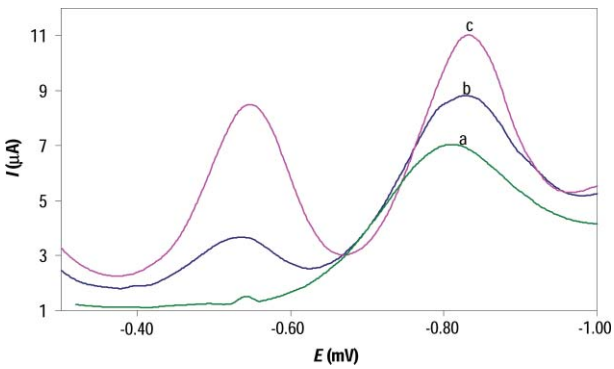

Fig. 7 Differential pulse voltammograms of 1 mM [Fe(L3)Cl] before (a) and after addition of 1 mM H_2DBC (b) and 2 mM Et_3N (c) in DMF at 25 °C. Supporting electrolyte: 0.1 M TBAP; Scan rate: 5 mV s^{-1}; Reference electrode: Ag/Ag^+; working electrode: Pt sphere.

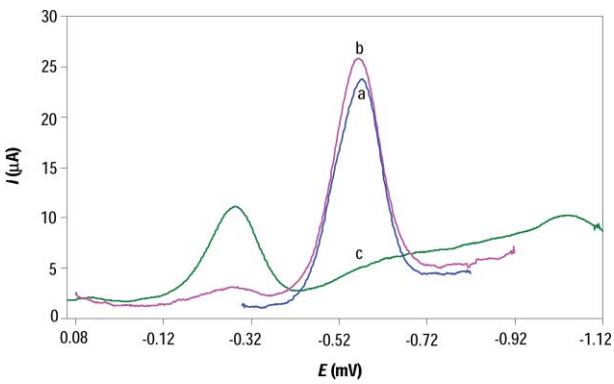

Fig. 8 Differential pulse voltammograms of 1 mM [Fe(L2)(H_2O)Cl] before (a) and after addition of 1 mM H_2DBC (b) and 2 mM Et_3N (c) in DMF at 25 °C. Supporting electrolyte: 0.1 M TBAP; Scan rate: 5 mV s^{-1}; Reference electrode: Ag/Ag^+; working electrode: Pt sphere.

Table 5 Electrochemical data[a] for the Fe^{III}/Fe^{II} redox process of iron(III) complexes and their DBC^{2-} adducts[b] in DMF at 25 ± 0.2 °C obtained using scan rates of 50 mV s^{-1} (CV) and 5 mV s^{-1} (DPV)

Compound	E_{pc}/V	E_{pa}/V	ΔE_p/mV	$E_{1/2}$/V		Redox process
				CV	DPV	
[Fe(L1)Cl]	–0.931	–0.680	251	–0.805	–0.808	$Fe^{III} \rightarrow Fe^{II}$
+ DBC^{2-}	–0.977	–0.843	134	–0.910	–0.932	$Fe^{III} \rightarrow Fe^{II}$ + LR
	–0.573	–0.465	108	–0.519	–0.522	DBSQ→H_2DBC
[Fe(L2)Cl(H_2O)][c]	–0.624	–0.540	84	–0.582	–0.577	$Fe^{III} \rightarrow Fe^{II}$
+ H_2DBC	–0.642	–0.534	108	–0.588	–0.579	$Fe^{III} \rightarrow Fe^{II}$
	–0.326	–0.246	80	–0.286	–0.279	DBSQ → H_2DBC
+ DBC^{2-}	–0.874	—	—	—	–1.020	$Fe^{III} \rightarrow Fe^{II}$ + LR
	–0.330	–0.218	112	–0.274	–0.285	DBSQ → H_2DBC
[Fe(L3)Cl]	–0.909	–0.759	150	–0.834	–0.836	$Fe^{III} \rightarrow Fe^{II}$
+ H_2DBC	–0.877	–0.781	96	–0.829	–0.850	$Fe^{III} \rightarrow Fe^{II}$ + LR
	–0.615	–0.533	82	–0.574	–0.560	DBSQ → H_2DBC
+ DBC^{2-}	–0.901	–0.861	40	–0.881	–0.850	$Fe^{III} \rightarrow Fe^{II}$ + LR
	–0.601	–0.513	96	–0.557	–0.568	DBSQ → H_2DBC
[Fe(L4)Cl]	–1.164	–0.996	168	–1.080	–1.010	$Fe^{III} \rightarrow Fe^{II}$
+ DBC^{2-}	–1.416	–1.152	264	–1.284	–1.308	$Fe^{III} \rightarrow Fe^{II}$ + LR
	–0.737	–0.573	164	–0.655	–0.645	DBSQ → H_2DBC

[a] Potential measured *vs.* $Ag/AgNO_3$ (0.01 M, 0.1 M TBAP); add 0.544 V to convert to NHE. [b] Generated by adding two equivalents Et_3N to H_2DBC. LR = ligand reduction.

Fe(III)/Fe(II) redox potential ($E_{1/2}$, –0.577 V) becomes more positive suggesting the enhancement in Lewis acidity of the iron(III) center as expected. Upon incorporation of one more methyl group at the *ortho* position of the phenolate arm in **1** to obtain **3** and upon replacement of the methyl groups in **3** by the more electron-releasing *tert*-butyl groups to form **4** the Fe(III)/Fe(II) redox potential becomes more negative reflecting the decrease in Lewis acidity of the iron(III) center.

On adding one equivalent of H_2DBC to **1**, **3** and **4** in DMF the Fe(III)/Fe(II) redox wave becomes intense suggesting the superposition of the redox wave corresponding to DBSQ/H_2DBC (DBSQ = di-*tert*-butylsemiquinone) couple[21–25,31] on it. And only for **2** and **3** a less intense new redox wave at potentials ($E_{1/2}$: **2**, –0.279; **3**, –0.560 V, Fig. 7, 8) more positive than the Fe(III)/Fe(II) redox wave appears. On adding two equivalents of Et_3N the Fe(III)/Fe(II) redox wave disappears,[31] which is shifted to a more negative potential (–0.850 to –1.308 V) for all the complexes illustrating formation of higher amounts of the adducts and the redox potential of DBSQ/DBC^{2-} couple ($E_{1/2}$: **1**, –0.522; **2**, –0.285; **3**, –0.568; **4**, –0.645 V, Fig. 7, 8) becomes considerably more positive than that of free DBSQ/H_2DBC couple (–1.434 V)[50] reflecting the significant stabilization of DBC^{2-} towards oxidation upon coordination to iron(III). The DBSQ/H_2DBC reduction wave for **2** appears even in the absence of Et_3N suggesting the spontaneous deprotonation of H_2DBC due to the strong affinity of catecholate anions to iron(III) with a higher Lewis acidity. Also, interestingly, the DBSQ/H_2DBC redox couple for **2** appears at a potential ($E_{1/2}$, –0.285 V, Fig. 8, Table 5) more positive than those for **1**, **3** and **4** ($E_{1/2}$: –0.522 to –0.645 V, Table 5) and the Fe(III) → Fe(II) redox wave disappears. This shows that DBC^{2-} bound to **2** is stabilized towards oxidation much more strongly than that bound to **1**, **3** and **4** and that the iron(III)-bound substrate in **2** is activated much more than that in **1**, **3** and **4** but much less than that in the previously reported $[Fe(N_4)Cl_2]^+$ complexes ($E_{1/2}$, –0.065 to –0.079 V).[34] The DBC^{2-} anion coordinated strongly to **2** has a tendency to lose electrons to form benzoquinone more readily than that coordinated weakly to **1**, **3** and **4**.

Catechol dioxygenase activity of iron(III) complexes

When the 3,5-di-*tert*-butylcatecholate (DBC^{2-}) adducts of all the complexes were generated *in situ* in DMF solution by reacting the complexes with H_2DBC pretreated with two equivalents of Et_3N/piperidine and their reactivity towards O_2 was investigated by monitoring the decay of the catecholate-to-iron(III) LMCT band (**1**, 530; **2**, 656; **3**, 541; **4**, 539 nm). The adducts of all the complexes are found to react as observed from the decrease in absorbance of the catecholate-to-iron(III) LMCT band. The pseudo-first order rate constants (k_{obs}: pip: 0.32–3.96 × 10^{-4} s^{-1}; Et_3N: 0.20–7.43 × 10^{-4} s^{-1}, Table 6) were calculated using equation (1) by fitting the decrease in intensity of the LMCT band into the following equation[31,51] applicable for relatively slow reactions,

$$A = A_\infty + (A_0 - A_\infty) \times \exp(-k_{obs} \times t) \quad (1)$$

$$k_{obs} = 1 + \log(\text{Abs}) \quad (2)$$

where, t is time, A, A_0 and A_∞ are the absorbances at time t, 0 and ∞ respectively and k_{obs} is the pseudo-first order rate constant and the $t_{1/2}$ of the catecholate adducts were calculated[31] using the equation $t_{1/2} = 0.693/k_{obs}$. The second order rate constants of the reactions were then derived (Pip: 0.66–9.60 × 10^{-2} M^{-1} s^{-1}; Et_3N: 0.41–15.28 × 10^{-2} M^{-1} s^{-1}) using the equation k_{o_2}(= $k_{obs}/[O_2]$. Interestingly, a new band around 400 nm appears and grows in intensity during oxygenation reaction of the DBC^{2-} adducts of **1**, **3** and **4**; however, no such band is discerned for the adduct of **2** as it is masked (*cf.* below) possibly by the absorption bands of ligand $–NO_2$ group. The oxygenation products were identified by GC-MS (EI) and quantified by GC (FID) techniques. It may be noted that catechols are also fragmented into unstable species, which are difficult to detect and characterized using GC-MS. When the DBC^{2-} adducts of **1–4** generated *in situ* using Et_3N as base were reacted with dioxygen in DMF solution over 48 h ($t_{1/2}$: pip: 0.49–6.02 h; Et_3N: 0.32–9.63 h) the simple two-electron oxidation product di-*tert*-butylbenzoquinone (DBQ) **11** is obtained in higher amounts for all the complexes (Et_3N: 6.4–26.1%; pip: 3.0–16.0%) and the

Table 6 Kinetic data for the oxidative cleavage of H_2DBC catalyzed by iron(III) complexes with O_2 in acetonitrile–DMF and the cleavage products analyzed after 48 h (see Scheme 3)

Complex[a]	Solvent	Base	Cleavage product (%)[b] Product (%)[b]	k_{obs} (10^{-4} s^{-1})	k_{O_2}(10^{-2} M^{-1} S^{-1})[c]	$t_{1/2}$ (h)[d]
[Fe(L1)(DBC)]$^-$	CH_3CN	Et_3N	**11** (27.2) **12** (1.5) **14** (1.4)	6.7 ± 0.5 2.3 ± 0.3[e]	8.2 ± 0.6	0.29
	CH_3CN	Pip	**11** (5.8) **12** (3.7) **14** (2.1)	8.0 ± 0.3 2.0 ± 0.1[e]	9.9 ± 0.4	0.24
	DMF	Et_3N	**11** (25.0) **12,13** (1.5)	7.4 ± 0.1 15.3 ± 0.3[e]	15.3 ± 0.2	0.25
	DMF	Pip	**11** (9.0) **12,13** (1.5) **14** (1.4)	4.7 ± 0.1 9.6 ± 0.1[e]	9.6 ± 0.1	0.41
[Fe (L2)(DBC)]$^-$	DMF	Et_3N	**11** (6.4) **12,13** (1.0)	0.2 ± 0.1	0.4 ± 0.1	9.63
	DMF	Pip	**11** (16.0) **12,13** (1.0) **14** (<1.0)	0.4 ± 0.1	0.9 ± 0.1	5.06
[Fe (L3)(DBC)]$^-$	CH_3CN	Et_3N	**11** (25.8) **12** (1.5) **14** (1.2)	2.7 ± 0.1 0.4 ± 0.1[e]	3.4 ± 0.1	0.70
	CH_3CN	Pip	**11** (6.2) **12** (3.2) **14** (1.7)	5.1 ± 0.2 0.3 ± 0.1[e]	6.3 ± 0.2	0.38
	DMF	Et_3N	**11** (26.1) **12,13** (<1.0) **14** (<1.0)	6.1 ± 1.4 0.5 ± 0.3[e]	12.5 ±3.0	0.32
	DMF	Pip	**11** (3.0) **12,13** (10.8) **14** (1.0)	4.0 ± 0.3 0.5 ±0.1[e]	8.2 ± 0.7	0.49
[Fe (L4)(DBC)]$^-$	CH_3CN	Et_3N	**11** (25.7) **12** (1.3)	0.2 ± 0.1 0.1 ±0.0[e]	0.3 ±0.1	8.75
	CH_3CN	Pip	**11** (19.6) **12** (2.3) **14** (1.0)	1.2 ±0.1	1.5 ±0.0	1.62
	DMF	Et_3N	**11** (23.46) **12,13** (1.34) **14** (<1.0)	1.0 ± 0.3 0.2 ± 0.0[e]	2.0 ± 0.6	2.06
	DMF	Pip	**11** (16.0) **12,13** (10.8) **14** (1.1)	0.3 ± 0.0 0.2 ± 0.0[e]	0.7 ± 0.1	6.02

[a] Generated by adding two equivalents of Et_3N and Piperidine, [b] Based on H_2DBC, [c] $k_{O_2} = k_{obs}/[O_2]$, [d] $t_{1/2} = 0.693/k_{obs}$, [e] Rate constant 3,5-di-*tert*-butylbenzoquinone formation (k'_{obs}), Pip = Piperidine.

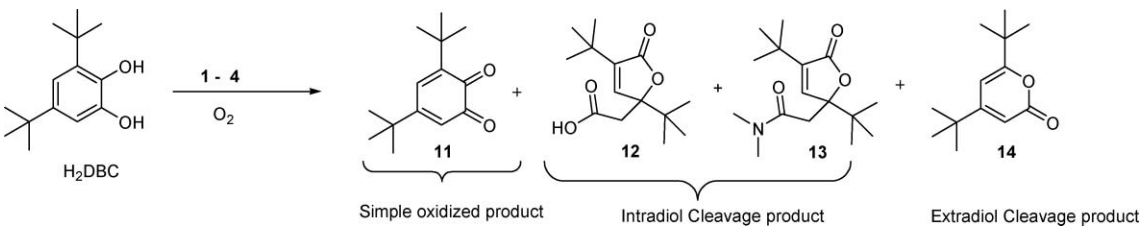

Scheme 3 Oxygenation products of H_2DBC for iron(III) complexes.

intradiol cleavage products 3,5-di-*tert*-butyl-5-(carboxymethyl)-2-furanone **12**, $C_{15}H_{24}O_4$, *m*/*z*, 254, and 3,5-di-*tert*-butyl-5-(*N*,*N*-dimethylamidomethyl)-2-furanone **13** (Et_3N: <1–1.5%; pip: 9.0–10.8%, Scheme 3, Table 6) and the extradiol cleavage products 4,6-di-*tert*-butyl-2-pyrone **14** were also obtained but in very small quantities (Et_3N: 0.0 – <1.0%; pip: <1.0–1.4%, Scheme 3). So, the band appearing around 400 nm and growing in intensity is ascribed[52] to the formation of **11** and the k_{obs}' values calculated for **1** and **3** from the increase in intensity of the band using equation (2) represent the rate of formation of DBQ (k_{obs}': Pip: 0.02–0.48 × 10^{-4} s^{-1}; Et_3N; 0.02–1.77 × 10^{-4} s^{-1}, Table 6) and the changes observed for **4** are not sufficiently good to calculate the rates. The intradiol cleavage products **12** and **13** are derived[53] from the nucleophilic attack of methoxide ion on *cis*,*cis*-muconic anhydride, which is the immediate product of oxidative cleavage.

The DBC^{2-} adducts of **1**, **3** and **4** were generated *in situ* in acetonitrile solution also and their reactivity towards O_2 was investigated as described above by monitoring the decay of the

DBC^{2-}-to-iron(III) LMCT band (**1**, 548; **3**, 540; **4**, 538 nm, Fig. 9). As complex **2** is insoluble in acetonitrile its reactivity was not investigated. The rate constant for oxygenation reaction of the complexes **1**, **3** and **4** (k_{o_2}: pip: 1.47–9.87 × 10^{-2} M^{-1} s^{-1}; Et_3N: 0.27–8.23 × 10^{-2} M^{-1} s^{-1}; Table 6) and the $t_{1/2}$ values of the catecholate adducts were calculated[31] as described above. The *in situ* generated adducts of **1**, **3** and **4** react with dioxygen in acetonitrile solution over 48 h ($t_{1/2}$: pip: 0.24–1.62 h; Et_3N: 0.29–8.75 h) to afford DBQ **11** as the simple two-electron oxidation product (Et_3N: 25.7–27.2%, pip: 5.8–19.6%, Scheme 3) and small amounts of both intradiol (Et_3N: 1.3–1.5%; pip: 2.3–3.7%) and extradiol cleavage products (Et_3N: 0–1.4%; pip: 1.0–2.1%) also.

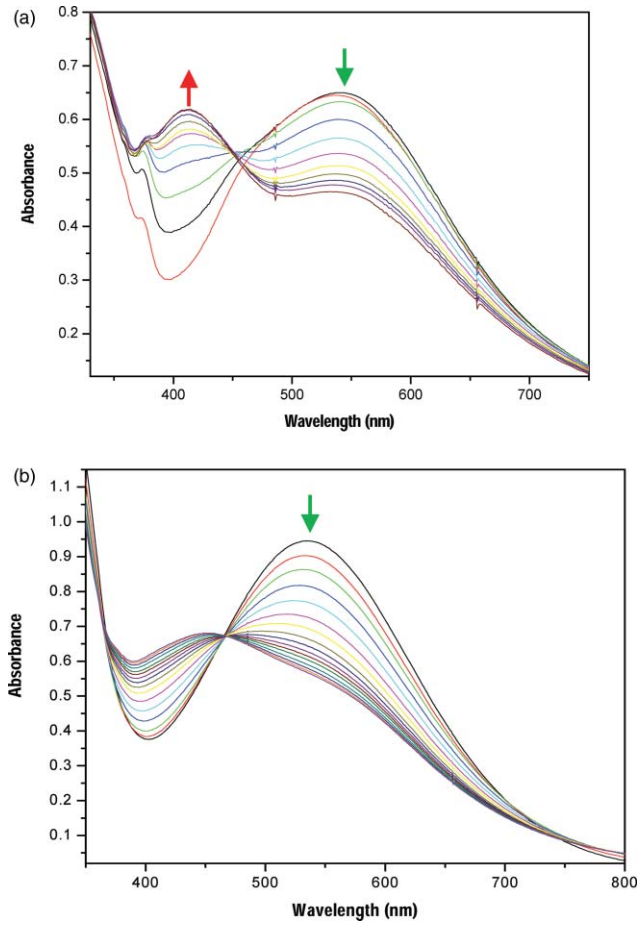

Fig. 9 (a) Electronic absorption spectral changes observed during the reaction of the adduct $[Fe(L3)(DBC)]^-$ generated *in situ* using Et_3N with O_2 at 25 °C in CH_3CN (2 × 10^{-4} M). (b) Electronic absorption spectral changes observed during the reaction of the adduct $[Fe(L3)(DBC)]^-$ generated *in situ* using piperidine with O_2 at 25 °C in CH_3CN (2 × 10^{-4} M).

The benzoquinone product for **1–4** in DMF/Et_3N is almost exclusive (6.4–26.1%) with only smaller amounts of intradiol (<1–1.5%) and extradiol cleavage products (0.0–1.0%) and a higher amount of benzoquinone (25.7–27.2%) is observed for **1**, **3** and **4** in acetonitrile/Et_3N solution. Similar formation of quinone as well as intradiol cleavage products has been observed for [Fe(SSCTH)(Cat)], where SS-CTH = (SS)-5,5,7,12,12,14-hexamethyl-l,4-,8,11-tetraazacyclo-tetradecane, in which the catecholate anion is coordinated in a monodentate fashion but no explanation was tendered for the observation.[54] Funabiki *et al.* have found[55] that when $FeCl_3$/BPY/Py was used for dioxygenation of catechol in THF solution the oxidized product benzoquinone was mainly obtained. Very recently, we have observed the formation of benzoquinone product in major amounts for the iron(III) complexes of tripodal tris(pyrazolyl)methane ligands.[56] The formation of benzoquinone product for the present complexes is illustrated by invoking molecular oxygen attack on the vacant iron(III) site in the five-coordinate adduct (a, Scheme 4; *cf.* above) in which DBC^{2-} is coordinated in bidentate fashion, as evidenced by spectral and electrochemical results (*cf.* above). As the bound O_2 molecule is located in the same plane as that of the catecholate substrate, it cannot attack the latter; however, it accepts two electrons from the bound substrate through iron(III) to for the quinone.[56] It is to be noted that one of the phenolate arms in the DBC^{2-} adduct remains uncoordinated because of steric constraint from the diazapane back bone, as revealed by molecular model building studies (*cf.* above). The re-coordination of the bulky *t*-butylphenolate arm displaced upon substrate binding is rendered difficult as it sterically clashes with the *t*-butyl group on the catecholate substrate, as revealed by building molecular models, leading to facilitate the attack of O_2 on the vacant iron(III) site and hence the amount of quinone product obtained for **4** in DMF–acetonitrile solution using piperidine as base is higher than those for **1** and **3**. However, when Et_3N is used as base all the adducts, except that of **2**, yield a higher amount of the quinone product in the same range suggesting that strong bidentate coordination effected by using piperidine encourages cleavage products. In contrast to **1**, **3** and **4**, a major amount of quinone product is observed for **2** in DMF/piperidine with smaller amounts of catechol cleavage products, which is consistent with the observation of its DBSQ/DBC^{2-} redox couple at a potential more positive than those for the other complexes (*cf.* above). As the displaced nitrophenolate arm in the catecholate adduct of **2** remains mostly uncoordinated to iron(III) the probability of molecular oxygen attacking the vacant iron(III) site is very high leading to the formation of quinone in major amounts.

When dioxygen attacks the activated carbon atom of catecholate substrate strongly bound to the iron(III) center in the adduct (substrate-activation mechanism), the Criegee intermediate $[(L)(DBSQ)Fe(III)O_2]^-$ gives intradiol cleavage products upon acyl migration and extradiol cleavage products upon alkenyl migration[44,57,58] (b, Scheme 4). On the other hand, when dioxygen attacks the iron(III) site of the DBC^{2-} adduct, vacated by the phenolate donor *cis* to both the catecholate oxygen atoms (oxygen-activation mechanism[18–26,29,34]) the same substrate-alkylperoxo-Fe^{3+} intermediate is formed leading to the yield of extradiol cleavage products (c, Scheme 4). The displacement of the second coordinated phenolate oxygen atom and hence the formation of the intermediate $[(L)(DBSQ)Fe(III)O_2]^-$ responsible for catechol cleavage does not appear to be facile and hence the observed formation of smaller amounts of the cleavage products. Also, it may be noted that the catecholate substrate, as it is weakly bound to the present bis(phenolate)iron(III) complexes with decreased Lewis acidity and hence insufficiently activated, is not prone to attack by free or iron(III)-bound dioxygen leading to smaller amounts of intradiol or extradiol cleavage products. The amounts of cleavage products obtained are higher and that of quinone product lower in DMF/piperidine than those respectively in acetonitrile/piperidine. The catecholate substrate is strongly

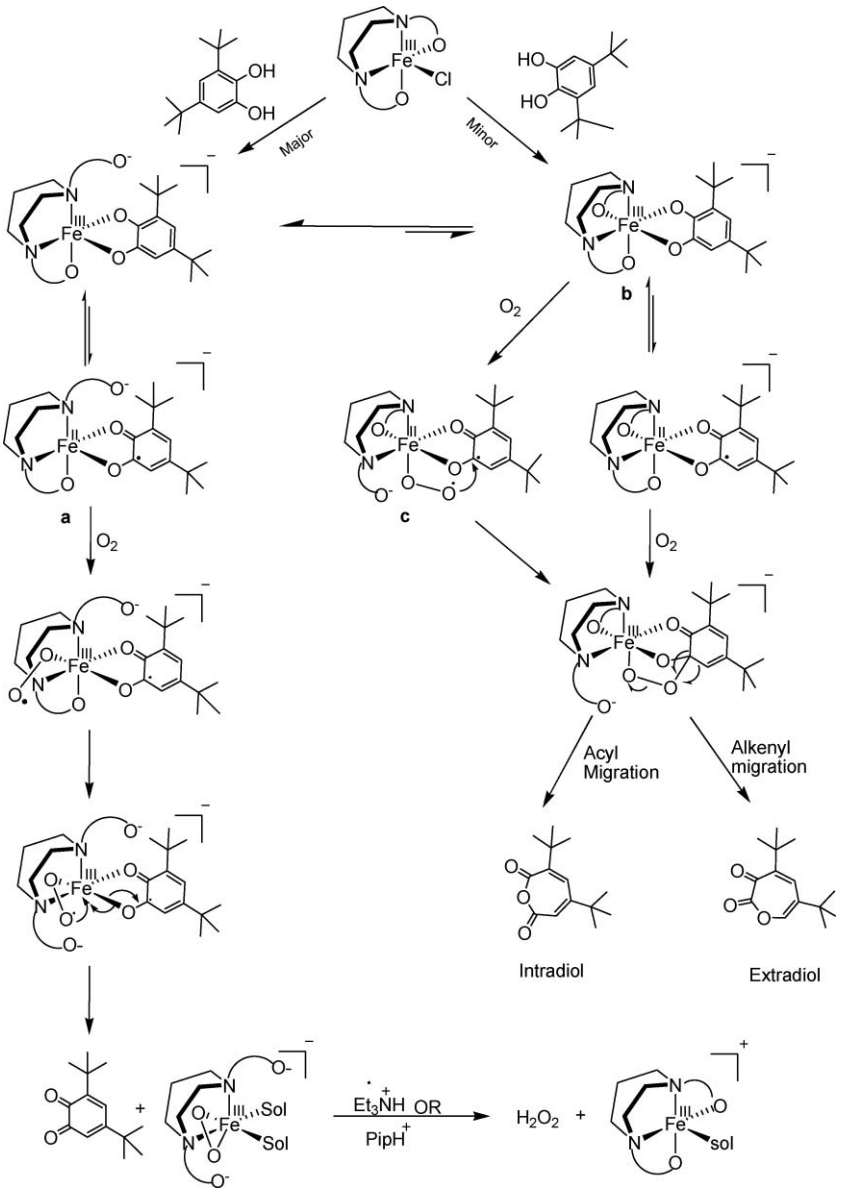

Scheme 4 Proposed reaction mechanism for H_2DBC oxidation and intradiol-cleavage catalyzed by **1–3**.

bound and hence activated in the coordinating solvent DMF more than in acetonitrile leading to the formation of higher amounts of intradiol cleavage products in DMF. However, when Et_3N is used as base the amount of quinone product obtained in DMF falls in the same range as that in acetonitrile. Also, in both DMF and acetonitrile solvents the amounts of cleavage products obtained are higher and that of quinone product lower when piperidine is used as base than when Et_3N is used as base. This is because a higher amount of six-coordinate complex is formed in the presence of the strong base piperidine. Also, interestingly, the ratio of the amount of intradiol cleavage product to that of quinone product observed for **1** and **3** is higher than that for **4** in DMF/piperidine. Obviously, the catecholate substrate is bound to the former complexes more strongly than to the latter and so molecular oxygen binds to adducts of the former complexes more strongly leading to a higher amount of intradiol cleavage product (*cf.* below). This is consistent with the observation of the DBSQ/DBC^{2-} redox couple for **4** at a potential more negative than for **1** and **3**.

As a major amount of quinone is mainly obtained for **1–4** (6.4–26.1%) in both DMF and acetonitrile solutions, it is evident that the observed rates of oxygenation correspond to mostly formation of quinone. The second order reaction rate constant (k_{o_2}, 1.9–15.3×10^{-2} M^{-1} s^{-1}, Table 6) for the adducts $[Fe(L)(DBC)]^-$ derived from **1**, **3** and **4** in DMF/Et_3N/piperidine are higher than that (k_{o_2}, $0.41–0.78 \times 10^{-2}$ M^{-1} s^{-1}) for the adduct of **2**. As DBC^{2-} is bound to iron(III) in $[Fe(L2)(DBC)]^-$ more strongly than in the adducts of the former complexes, as revealed by the more positive $E_{1/2}$ value of DBSQ/DBC^{2-} couple (*cf.* above), the electron-transfer from bound catecholate to dioxygen is rendered difficult and hence the lower rates of quinone formation for **2**. This is consistent with the relatively low yields of the quinone product for **2** when Et_3N is used as base (*cf.* above). Interestingly, the rate of quinone formation decreases in the order, **1** > **3** > **4** in both acetonitrile

and DMF when Et_3N or piperidine is used as base. The increase in molecular crowding in the complexes along this series would discourage the attack of molecular oxygen on the vacant iron(III) site. Also, as the Lewis acidity of the iron(III) center decreases along this series (*cf.* electrochemical studies), the extent of interaction of the catecholate substrate and hence the rate of oxygenation of these complexes would decrease in the above order. Interestingly, a higher rate of quinone formation is observed for complexes with a higher LMCT band energy suggesting stronger interaction of catecholate with iron(III) center confers higher reactivity. This is similar to that observed for the catechol cleavage reactions.[31,34] Further, the DBC^{2-} adducts of the present iron(III)-bis(phenolate) complexes undergo dioxygenation much more slowly than those for the analogous iron(III) complexes of pyridyl-based iron(III)-N4 ligands,[34] which is due to the lower Lewis acidity and hence the weaker interaction of **1–4** with the catecholate substrate. However, they undergo oxygenation with rates faster than the previously reported iron(III)-bis(phenolate) complexes,[21] which is consistent with the higher Fe–O–C bond angle (135.5°) observed for one of them (**3**). Also, it may be noted that the trigonal bipyramidal and octahedral iron(III)-phenolate complexes having the Fe–O–C bond angle of ~128.5° have been reported to show slow or no dioxygenase activity.[21,22] Further, interestingly, the rate of dioxygenation for **1**, **3** and **4** in DMF is higher than that in acetonitrile. The enhanced bidentate coordination of catechol in DMF leads to faster electron transfer from catecholate adduct to iron(III)-bound O_2. However, this trend is not observed when piperidine is used as base because cleavage reactions are also facilitated in the presence of the strong base used. Also, for all the complexes the rate of dioxygenation is dependent on the base used; thus they are higher in the presence of Et_3N than in piperidine because of the occurrence of cleavage reactions, which contribute to the observed rates of reactions. In fact, when the weak base Et_3N is used, interestingly, the oxidized product is obtained in very large quantities with the cleavage products in smaller quantities.

Thus, the subtituents on the present bis(phenolate) ligands determine the Lewis acidity of the iron(III) center in the complexes, and also the ability of the ligands to rearrange to accommodate the chelating catecholate substrate, and dictate the extent of interaction of the complexes with catechol and hence the type of reaction of catechol—quinone formation *vs.* catechol cleavage—and also the rate of formation and amount of cleavage/quinone product formed. Thus the iron(III) complex of a weakly coordinating primary bis(*p*-NO_2-phenolate) ligand tends to yield the oxidized product in major amounts while that of the sterically crowded bis(di-*t*-butylphenolate) ligand yields the quinone as well as an enhanced amount of intradiol cleavage product in the presence of a strong base.

Conclusions and relevance to catechol dioxygenases

A few novel iron(III) complexes of bis(phenolate) ligands with diazepane back bone have been isolated and studied as structural and functional models for intradiol-cleaving catechol dioxygenases. One of these complexes with two 3,5-dimethylphenolate donors possesses a novel square pyramidal coordination geometry with structural parameters (Fe–$O_{phenolate}$, 1.855 Å; Fe–O–C, 135.5°) close to those for the intradiol-cleaving 3,4-PCD enzymes (Fe–O_{tyr}, 1.81, 1.91 Å; Fe–O–C, 133, 148°) and the iron(III) complexes with methyl- and 3,5-di-*tert*-butyl substituents on the phenolate rings also exhibit a similar coordination geometry. In contrast, the analogous bis(*p*-nitrophenolate) complex possesses an octahedral coordination geometry. In DMF/Et_3N all the complexes elicit the two-electron oxidation of the model substrate 3,5-di-*tert*-butylcatechol (H_2DBC) to give a major amount of benzoquinone and smaller amounts of both intra- and extradiol cleavage products. However, interestingly, when piperidine is used as base a decrease in the amount of oxidation product with an increase in catechol cleavage product is achieved. Thus the extent of interaction of the bis(phenolate) complexes with catechol and the catechol cleavage activities and/or the two-electron oxidation of the catechol as well are dictated by the Lewis acidity of the iron(III) center of the bis(phenolate) complexes, as fine-tuned by the nature of substituents on the phenolate rings, the solvent and base as well. This study reveals that catechol cleavage can be achieved and catechol oxidation prevented by tuning the ligand architecture by incorporating strongly coordinating ligand donors and by using a coordinating solvent and a stronger base to encourage the bidentate coordination of catechol. The displacement of one of the two coordinated phenolate donors from the iron(III) coordination sphere upon catecholate binding is followed by molecular oxygen attack at the same site leading to the formation of quinone product. Such a displacement of the phenolate donor is interestingly similar to that observed for the 1,2-CTD dioxygenase upon binding to the catechol substrate; however, only the quinone is formed as the site of attack of dioxygen is located in the plane of the catecholate substrate.

Acknowledgements

We sincerely thank the Department of Science and Technology, New Delhi for supporting this research [Scheme No. SR/S5/BC-05/2006], and the Council of Scientific and Industrial Research, New Delhi for a Senior Research Fellowship to R. M. Professor M. Palaniandavar is a recipient of a Ramanna Fellowship of Department of Science and Technology, New Delhi. We thank Professor P. Sambasiva Rao, Pondicherry University for providing the EPR facility.

Notes and references

1 A. L. Feig and S. J. Lippard, *Chem. Rev.*, 1994, **94**, 759–805.
2 E. L. Hegg and L. Que, Jr., *Eur. J. Biochem.*, 1997, **250**, 625–629.
3 J. D. Lipscomb and A. M. Orville, in *Degradation of Environmental Pollutants by Microorganisms and Their Metalloenzymes*, H. Sigel, A. Sigel, ed. Marcel Dekker: New York, 1992, Vol. 28, pp 243–298.
4 (*a*) L. Que, Jr. and R. Y. N. Ho, *Chem. Rev.*, 1996, **96**, 2607–2624; (*b*) M. Abu-Omar, A. Loaiza and N. Hontzeas, *Chem. Rev.*, 2005, **105**, 2227–2252.
5 E. I. Solomon, T. Brunold, M. I. Davis, J. N. Kemsley, S. K. Lee, N. Lehnert, F. Neese, A. J. Skulan, Y. S. Yang and J. Zhou, *Chem. Rev.*, 2000, **100**, 235–349.
6 S. Dagley, In *The Bacteria*, J. R. Sokatch and L. N. Ornston, ed.; Academic Press: Orlando, 1986 Vol. 10, Chapter 10, pp 527–555.
7 M. A. Levin and M. A. Gealt, in *Biotreatment of Industrial and Hazardous Waste*, M. A. Levin and M. A. Gealt, ed.; McGraw-Hill, New York, 1993, pp 5–7.
8 L. Que, Jr., J. D. Lipscomb, E. Münck and J. M. Wood, *Biochim. Biophys. Acta*, 1977, **485**, 60–74.
9 (*a*) L. Que, Jr., In *Iron Carriers and Iron Proteins*, T. M. Loehr, ed. VCH: New York, 1989, pp 467–524; (*b*) L. Shu, Y.-M. Chiou, A. M. Miller, J. D. Lipscomb and L. Que, Jr., *Biochemistry*, 1995, **34**, 6649–6659.
10 D. H. Ohlendorf, J. D. Lipscomb and P. C. Weber, *Nature*, 1988, **336**, 403–405.

11 D. H. Ohlendorf, A. M. Orville and J. D. Lipscomb, *J. Mol. Biol.*, 1994, **244**, 586–608.
12 M. P. Valley, C. K. Brown, D. L. Burk, M. W. Vetting, D. H. Ohlendorf and J. D. Lipscomb, *Biochemistry*, 2005, **44**, 11024–11039.
13 R. W. Frazee, A. M. Orville, K. B. Dolbeare, H. Yu, D. H. Ohlendorf and J. D. Lipscomb, *Biochemistry*, 1998, **37**, 2131–2144.
14 (*a*) M. W. Vetting, D. A. D' Argenio, L. N. Ornston and D. H. Ohlendorf, *Biochemistry*, 2000, **39**, 7943–7955; (*b*) T. E. Elgren, A. M. Orville, K. Kelly, J. D. Lipscomb, D. H. Ohlendorf and L. Que, Jr., *Biochemistry*, 1997, **36**, 11504–1513.
15 M. W. Vetting and D. H. Ohlendorf, *Structure*, 2000, **8**, 429–440.
16 (*a*) J. W. Whittaker and J. D. Lipscomb, *J. Biol. Chem.*, 1984, **259**, 4487–4495; (*b*) A. M. Orville and J. D. Lipscomb, *J. Biol. Chem.*, 1989, **264**, 8791–8801; (*c*) A. E. True, A. M. Orville, L. L. Pearce, J. D. Lipscomb and L. Que, Jr., *Biochemistry*, 1990, **29**, 10847–10854.
17 (*a*) A. M. Orville, J. D. Lipscomb and D. H. Ohlendorf, *Biochemistry*, 1997, **36**, 10052–10066; (*b*) A. M. Orville, N. Elango, J. D. Lipscomb and D. H. Ohlendorf, *Biochemistry*, 1997, **36**, 10039–10051.
18 M. Costas, M. P. Mehn, M. P. Jensen and L. Que, Jr., *Chem. Rev.*, 2004, **104**, 939–986.
19 M. I. Davies, A. M. Orville, F. Neese, J. M. Zaleski, J. D. Lipscomb and E. I. Solomon, *J. Am. Chem. Soc.*, 2002, **124**, 602–614.
20 R. Yamahara, S. Ogo, H. Masuda and Y. Watanabe, *J. Inorg. Biochem.*, 2002, **88**, 284–294.
21 M. Velusamy, M. Palaniandavar, R. Srinivasa Gopalan and G. U. Kulkarni, *Inorg. Chem.*, 2003, **42**, 8283–8293.
22 M. Velusamy, R. Mayilmurugan and M. Palaniandavar, *Inorg. Chem.*, 2004, **43**, 6284–6293.
23 M. Velusamy, R. Mayilmurugan and M. Palaniandavar, *J. Inorg. Biochem.*, 2005, **99**, 1032–1042.
24 H. G. Jang, D. D. Cox and L. Que, Jr., *J. Am. Chem. Soc.*, 1991, **113**, 9200–9204.
25 (*a*) R. Viswanathan and M. Palaniandavar, *J. Chem. Soc., Dalton Trans.*, 1995, 1259–1266; (*b*) R. Viswanathan, M. Palaniandavar, T. Balasubramanian and P. T. Muthiah, *Inorg. Chem.*, 1998, **37**, 2943–2951; (*c*) T. Dhanalakshmi, M. Bhuvaneshwari and M. Palaniandavar, *J. Inorg. Biochem.*, 2006, **100**, 1527–1534; (*d*) M. Palaniandavar, M. Velusamy and R. Mayilmurugan, *J. Chem. Sci.*, 2006, **118**, 601–610; (*e*) M. Palaniandavar and R. Mayilmurugan, *C. R. Chimie.*, 2007, **10**, 366–379; (*f*) K. Sundaravel, T. Dhanalakshmi, E. Suresh and M. Palaniandavar, *Dalton Trans.*, 2008, 7012–7025.
26 (*a*) M. Pascaly, M. Duda, A. Rompel, B. H. Sift, W. M. Klauckean and B. Krebs, *Inorg. Chim. Acta*, 1999, **291**, 289–299; (*b*) M. Pascaly, C. Nazikkol, F. Scweppe, A. Wiedeman, K. Zurlinden Muller and B. Krebs, *Z. Anorg. Allg. Chem.*, 2000, **626**, 50–55; (*c*) M. Duda, M. Pascaly and B. Krebs, *Chem. Commun.*, 1997, 835–836; (*d*) M. Merkel, M. Pascaly, B. Krebs, J. Astner, S. P. Foxon and S. Schindler, *Inorg. Chem.*, 2005, **44**, 7582–7589; (*e*) M. Merkel, D. Schindler, S. M. Baldeau and B. Krebs, *Eur. J. Inorg. Chem.*, 2004, (4), 783–790.
27 M. Merkel, F. K. Müller and B. Krebs, *Inorg. Chim. Acta*, 2002, **337**, 308–316.
28 M. Pascaly, M. Duda, F. Schweppe, F. Zurlinden, K. Muller and B. Krebs, *J. Chem. Soc., Dalton Trans.*, 2001, 828–837.
29 W. O. Koch and H.-J. Krüger, *Angew. Chem., Int. Ed. Engl.*, 1996, **34**, 2671–2674.
30 (*a*) L. S. White, P. V. Nilsson, L. H. Pignolet and L. Que, Jr., *J. Am. Chem. Soc.*, 1984, **106**, 8312–8313; (*b*) J. W. Pyrz, A. L. Roe, L. J. Stern and L. Que, Jr., *J. Am. Chem. Soc.*, 1985, **107**, 614–620; (*c*) T. Funabiki, H. Sakamoto, S. Yoshida and K. Tarama, *J. Chem. Soc., Chem. Commun.*, 1979, 754–755; (*d*) T. Funabiki, T. Yamazaki, A. Fukui, T. Tanaka and S. Yoshida, *Angew. Chem., Int. Ed.*, 1998, **37**, 513–515; (*e*) S. Ogo, R. Yamahara, T. Funabiki, H. Masuda and Y. Watanabe, *Chem. Lett.*, 2001, 1062–1063; (*f*) T. Funabiki, A. Fukui, Y. Hitomi, M. Higuchi, T. Yamamoto, T. Tanaka, F. Tani and Y. Naruta, *J. Inorg. Biochem.*, 2002, **91**, 151–158; (*g*) T. Funabiki, D. Sugio, N. Inui, M. Maeda and Y. Hitomi, *Chem. Commun.*, 2002, 412–413; (*h*) Y. Hitomi, M. Higuchi, T. Tanaka and T. Funabiki, *Inorg. Chim. Acta*, 2005, **358**, 3465–3470; (*i*) M. Higuchi, Y. Hitomi, H. Minami, T. Tanaka and T. Funabiki, *Inorg. Chem.*, 2005, **44**, 8810–8821; (*j*) J. H. Lim, H.-J. Lee, K.-B. Lee and H. G. Jang, *Bull. Korean. Chem. Soc.*, 1997, **18**, 1166–1171; (*k*) P. C. A. Bruijnincx, M. Lutz, A. L. Spek, W. R. Hagen, G. van Koten and R. J. M. Klein Gebbink, *Inorg. Chem.*, 2007, **46**, 8391–8402; (*l*) F. Li, M. Wang, P. Li, T. Zhang and L. Sun, *Inorg. Chem.*, 2007, **46**, 9364–9371; (*m*) N. Raffard, R. Carina, A. J. Simaan, J. Sainton, E. Riviere, L. Tchertanov, S. Bourcier, G. Bouchoux, M. Delroisse, F. Banse and J.-J. Girerd, *Eur. J. Inorg. Chem.*, 2001, 2249–2254.
31 (*a*) R. Mayilmurugan, E. Suresh and M. Palaniandavar, *Inorg. Chem.*, 2007, **46**, 6038–6049; (*b*) R. Mayilmurugan, K. Visvaganesan, E. Suresh and M. Palaniandavar, *Inorg. Chem.*, 2009, **48**, 8771–8783.
32 (*a*) R. B. Lauffer, R. H. II. Heistand and L. Que, Jr., *J. Am. Chem. Soc.*, 1981, **103**, 3947–3949; (*b*) R. H. II. Heistand, A. L. Roe and L. Que, Jr., *Inorg. Chem.*, 1982, **21**, 676–681; (*c*) R. H. II. Heistand, R. B. Lauffer, E. Fikrig and L. Que, Jr., *J. Am. Chem. Soc.*, 1982, **104**, 2789–2796; (*d*) R. B. Lauffer, R. H. II. Heistand and L. Que, Jr., *Inorg. Chem.*, 1983, **22**, 50–55.
33 (*a*) H. Fujii and Y. Funabashi, *Angew. Chem., Int. Ed.*, 2002, **41**, 3638–3641; (*b*) T. Kurahashi, K. Oda, M. Sugimoto, T. Ogura and H. Fujii, *Inorg. Chem.*, 2006, **45**, 7709–7721.
34 R. Mayilmurugan, H. S. Evans and M. Palaniandavar, *Inorg. Chem.*, 2008, **47**, 6645–6658.
35 R. Mayilmurugan, E. Suresh, H. S. Evans and M. Palaniandavar, *Dalton Trans.*, 2009, (26), 5101–5114.
36 (*a*) Japan Chemical Society, *Kagaku-Binran Basic Part II*, 2nd edition, Maruzen, Tokyo, 1975; (*b*) D. T. Sawyer, *Oxygen Chemistry*, Oxford University Press, New York, 1991.
37 P. Mialane, L. Tehertanov, F. Banse, J. Sainton and J. Girerd, *Inorg. Chem.*, 2000, **39**, 2440–2444.
38 *SMART & SAINT Software Reference manuals, version 5.0*, Bruker AXS Inc.: Madison, WI, 1998.
39 G. M. Sheldrick, *SADABS software for empirical absorption correction*University of Göttingen: Germany, 2000.
40 *SHELXTL Reference Manual, version 5.1*, Bruker AXS Inc., Madison, WI, 1998.
41 E. Y. Tshuva, I. Goldberg, M. Kol and Z. Goldschmidt, *Organometallics*, 2001, **20**, 3017–3028.
42 A. W. Addison, T. N. Rao, J. Reedijk, J. Van Rijn and G. C. Vershcoor, *J. Chem. Soc., Dalton Trans.*, 1984, 1349–1356.
43 M. R. McDevitt, A. W. Addision, E. Sinn and L. K. Thompson, *Inorg. Chem.*, 1990, **29**, 3425–3433.
44 K. Visvaganesan, R. Mayilmurugan, E. Suresh and M. Palaniandavar, *Inorg. Chem.*, 2007, **46**, 10294–10306.
45 (*a*) L. Casella, M. Gullotti, A. Pintar, L. Messouri, A. Rockenbauer and M. Gyor, *Inorg. Chem.*, 1987, **26**, 1031–1038; (*b*) S. Wang, L. Wang, X. Wang and Q. Luo, *Inorg. Chim. Acta*, 1997, **254**, 71–77; (*c*) B. Krebs, K. Schepers, B. Bremer, G. Henkel, E. Althus, W. Muller-Warmuth, K. Griesar and W. Haase, *Inorg. Chem.*, 1996, **35**, 2360–2368; (*d*) B. P. Gaber, V. Miskowski and T. G. Spiro, *J. Am. Chem. Soc.*, 1974, **96**, 6868–6873; (*e*) M. S. Shongwe, C. H. Kaschula, M. S. Adsetts, E. W. Ainscough, A. M. Brodie and M. J. Morris, *Inorg. Chem.*, 2005, **44**, 3070–3079; (*f*) C. Imbert, H. P. Hratchian, M. Lanznaster, M. J. Heeg, L. M. Hryhorczuk, B. R. McGarvey, H. B. Schlegel and C. Verani, *Inorg. Chem.*, 2005, **44**, 7414–7422.
46 D. D. Cox, S. J. Benkovic, L. M. Bloom, F. C. Bradley, M. J. Nelson, L. Que, Jr. and D. E. Wallick, *J. Am. Chem. Soc.*, 1988, **110**, 2026–2032.
47 A. J. Simaan, M.-L. Biollot, E. Riviere, A. Boussac and J.-J. Girerd, *Angew. Chem., Int. Ed.*, 2000, **39**, 196–198.
48 (*a*) M. R. Bukowshi, P. Comba, C. Limberg, M. Merz, L. Que, Jr. and T. Wistuba, *Angew. Chem., Int. Ed.*, 2004, **43**, 1283–1287; (*b*) S. Yoon, H.-J. Lee, K.-B. Lee and H. G. Jang, *Bull. Korean. Chem. Soc.*, 2000, **21**, 923–928.
49 A. J. Bard and L. R. Faulkner, *Electrochemical Methods: Fundamental and Applications*, John Wiley & Sons, New York, 1980pp 218.
50 E. J. Nanni, M. D. Stalling and D. T. Sawyer, *J. Am. Chem. Soc.*, 1980, **102**, 4481–4485.
51 Y. Hitomi, M. Yoshida, M. Higuchi, H. Minami, T. Tanaka and T. Funabiki, *J. Inorg. Biochem.*, 2005, **99**, 755–763.
52 Y. Hitomi, A. Ando, H. Matsui, T. Ito, T. Tanaka, S. Ogo and T. Funabiki, *Inorg. Chem.*, 2005, **44**, 3473–3478.
53 L. Que Jr., R. C. Kolanczyk and L. S. White, *J. Am. Chem. Soc.*, 1987, **109**, 5373.
54 A. Dei, D. Gatteschi and L. Pardi, *Inorg. Chem.*, 1993, **32**, 1389–1395.
55 T. Funabiki, A. Mizoguchi, T. Sugimoto, S. Tada, M. Tsugi, H. Sakamoto and S. Yoshida, *J. Am. Chem. Soc.*, 1986, **108**, 2921.
56 T. Dhanalakshmi, E. Suresh and M. Palaniandavar, *Dalton Trans.*, 2009, 8317–8328.
57 C. J. Winfield, Z. Al-Mahrizy, M. Gravestock and T. D. H. Bugg, *J. Chem. Soc., Perkin Trans. 1*, 2000, 3277–3289.
58 S. Mendel, A. Arndt and T. D. H. Bugg, *Biochemistry*, 2004, **43**, 13390–13396.